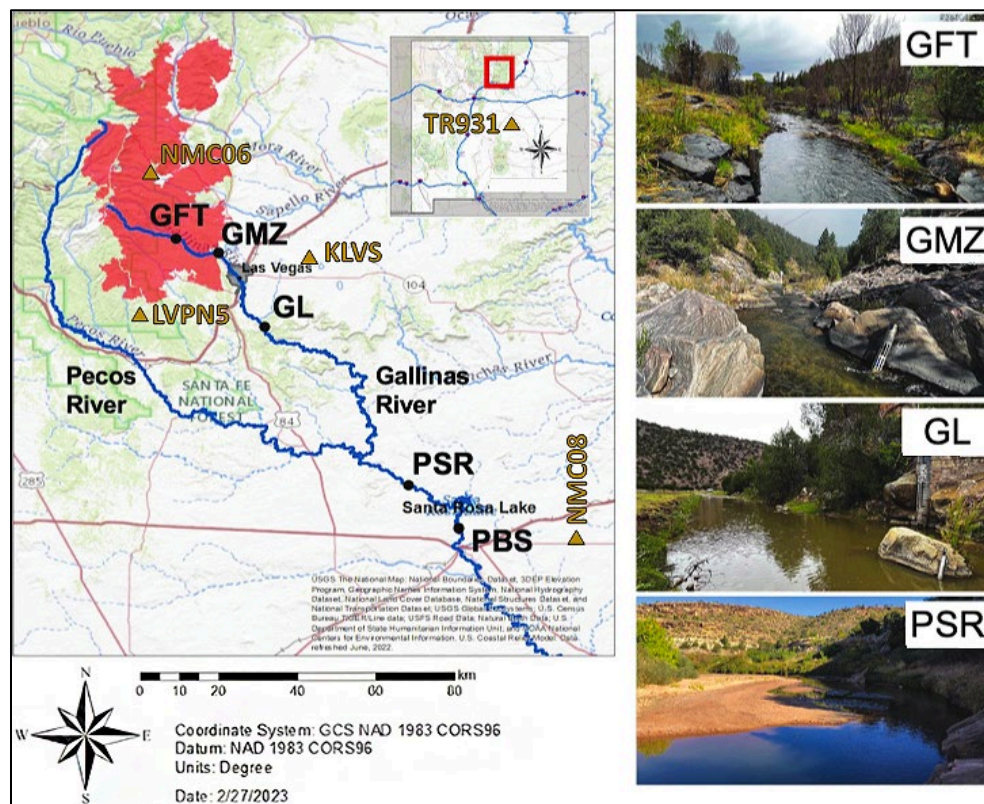


November 2023

QUANTIFYING THE LONGITUDINAL PROPAGATION OF AQUATIC DISTURBANCES FROM THE HERMIT'S PEAK/CALF CANYON FIRE ALONG THE GALLINAS CREEK-PECOS RIVER FLUVIAL NETWORK

NM WRI Technical Completion Report No. 407

Ricardo González-Pinzón
Paige Tunby
Justin Nichols
Asmita Kapfle
Aashish Khandelwal
David Van Horn



Site map of sensor deployment. Red highlighted region represents the burn boundary of the Hermit's Peak/Calf Canyon Fire.

New Mexico Water Resources Research Institute
New Mexico State University
MSC 3167, P.O. Box 30001
Las Cruces, New Mexico 88003-0001
(575) 646-4337 email: nmwri@nmsu.edu



QUANTIFYING THE LONGITUDINAL PROPAGATION OF AQUATIC DISTURBANCES
FROM THE HERMIT'S PEAK/CALF CANYON FIRE ALONG THE GALLINAS CREEK-
PECOS RIVER FLUVIAL NETWORK

By

Ricardo González-Pinzón, Associate Professor

Paige Tunby, Justin Nichols, Asmita Kaphle, and Aashish Khandelwal, Graduate Students

David Van Horn, Research Assistant Professor

Department of Civil, Construction and Environmental Engineering
University of New Mexico

TECHNICAL COMPLETION REPORT

Account Number EQ02305

Technical Completion Report 407

November 2023

New Mexico Water Resources Research Institute
in cooperation with the
Department of Plant & Environmental Sciences
New Mexico State University

The research on which this report is based was financed in part by the U.S. Department of the Interior, Geological Survey, through the New Mexico Water Resources Research Institute. This material is based upon work supported by the U.S. Geological Survey under Grant/Cooperative Agreement No. (G21AP10635).

DISCLAIMER

The purpose of the NM Water Resources Research Institute (NM WRRI) technical reports is to provide a timely outlet for research results obtained on projects supported in whole or in part by the institute. Through these reports the NM WRRI promotes the free exchange of information and ideas and hopes to stimulate thoughtful discussions and actions that may lead to resolution of water problems. The NM WRRI, through peer review of draft reports, attempts to substantiate the accuracy of information contained within its reports, but the views and conclusions contained in this document are those of the authors and should not be interpreted as representing the opinions or policies of the U.S. Geological Survey. Mention of trade names or commercial products does not constitute their endorsement by the U.S. Geological Survey.

ABSTRACT

Wildfires are increasing globally in frequency, severity, and extent, but their impact on fluvial networks, and the resources they provide, remains unclear. Growing evidence suggests that wildfires trigger cascading impacts that propagate across fluvial networks and impact key ecosystem services. These impacts originate in hillslopes and streams within burned areas and affect water quantity and quality over multiple spatiotemporal scales. While we currently map fire areas and their severity with relatively high accuracy using areal and satellite images, we do not have comparable abilities to map the propagation of wildfire disturbances across fluvial networks. Since current fire models consistently predict that the prevalence of wildfire and associated damage will continue to increase due to anthropogenic climate change and forest management practices, we must be able to quantify and predict the propagation of wildfire disturbances. However, to date, we lack data and modeling tools to answer the fundamental questions: How far downstream do wildfire disturbances propagate in fluvial networks and what are the key controlling factors? These knowledge gaps hinder our ability to mitigate wildfire impacts on aquatic ecosystems and to protect their vital services. We monitored the propagation of water quality disturbances generated by the largest wildfire recorded in New Mexico, the Hermit's Peak/Calf Canyon Fire. For this, we instrumented multiple sites along the Gallinas Creek – Pecos River fluvial network, and at Santa Rosa Lake. We found that burned material became available soon after the monsoon precipitation began and that such disturbances propagated for more than 180 km and were brought into Santa Rosa Lake, which regulated the propagation of sediments and ash. The work presented here is being submitted for peer-reviewed publication led by the graduate students working on the project. We appreciate your respect for their work.

Keywords: rapid response team, wildfires, water quality, sensors, streams

TABLE OF CONTENTS

DISCLAIMER	ii
ABSTRACT.....	iii
LIST OF FIGURES	v
LIST OF TABLES.....	vi
1. JUSTIFICATION OF WORK PERFORMED.....	1
2. REVIEW OF METHODS USED.....	3
2.1. Rapid Response Team (RRT) monitoring with sensors	3
2.1.1. Equipment used.....	3
2.1.2. Raw data conversions.....	5
2.1.3. Data quality control and assurance.....	6
2.1.4. Data Organization, Metabolic Modeling, and Statistical Methods	7
2.1.4.1. Periods of analysis	7
2.1.4.2. Stream Metabolism	7
2.1.4.3. Exceedance Probability.....	8
2.1.4.4. Principal component analysis	9
2.2. RRT monitoring with grab sampling.....	9
2.2.1. Sampling locations	9
2.2.2. Grab Sample Analysis.....	12
2.2.3. Quality control.....	13
2.3. RRT with The Navigator	14
3. DISCUSSION OF RESULTS AND THEIR SIGNIFICANCE	16
3.1. RRT monitoring with sensors	16
3.1.1. Pre-Monsoon period.....	16
3.1.2. Monsoon period.....	19
3.1.3. Post-Monsoon period	20
3.2. RRT monitoring with grab sampling.....	21
3.2.1. RRT monitoring with The Navigator	24
4. PRINCIPAL FINDINGS, CONCLUSIONS, AND RECOMMENDATIONS.....	27
4.1. Disturbance effects on surface water quality in streams and rivers	27
4.2. Disturbance effects on stream metabolism.....	31
4.3. Disturbance effects on lakes, and lake controls on propagation of disturbances	32
4.4. Disturbance effects on communities	34
5. REFERENCES	36

LIST OF FIGURES

Figure 1. Site map of sensor deployment. Red highlighted region represents the burn boundary of the Hermit’s Peak/Calf Canyon Fire.....	4
Figure 2. Grab sampling locations	11
Figure 3. Example of calibration curves from the test methods of different species.....	14
Figure 4. The Navigator monitoring water quality in Santa Rosa Lake (left), and the kayak with the multiparameter sonde monitoring the Pecos River (right).....	15
Figure 5. QA/QC timeseries data from EXO2 water quality sondes and weighted average precipitation from nearby climate stations. Data collected at A) Gallinas Creek near Gallinas, B) Gallinas Creek near Montezuma, C) Gallinas Creek near Lourdes, and Pecos River D) upstream and E) downstream of Santa Rosa Lake	16-18
Figure 6. Boxplots of QA/QC data from water quality sondes at each site from April 26, 2022, through November 8, 2022	20
Figure 7. Concentrations of ammonium from Gallinas Creek to Santa Rosa Lake.....	21
Figure 8. Concentrations of phosphate from Gallinas Creek to Santa Rosa Lake.....	22
Figure 9. Concentrations of sulphate from Gallinas Creek to Santa Rosa Lake.....	23
Figure 10. Concentrations of A) TON, B) nitrate, and C) nitrite from Gallinas Creek to Santa Rosa Lake.....	23-24
Figure 11. Lagrangian data of DO, specific conductivity, turbidity, pH, and water temperature collected with The Navigator. Data were collected during the monsoon period (green, blue, and red) and post-monsoon (orange). The red zone indicates the delta, which shifted as the lake level rose from 1432.51m to 1435.82m	26
Figure 12. Exceedance probability plots for A) Gallinas at Montezuma, B) Gallinas at Lourdes, C) Pecos River Upstream of Santa Rosa Lake, and D) Pecos River Downstream of Santa Rosa Lake. The four highest discharge events in 2022 are annotated on the plot	27-28
Figure 13. Principal component analysis at each sonde site from April 26, 2022, to November 8, 2022. A) Gallinas Creek near Gallinas, B) Gallinas Creek near Montezuma, C) Gallinas Creek near Lourdes, D) Pecos River upstream of Santa Rosa Lake, E) Pecos River downstream of Santa Rosa Lake.....	29-31
Figure 14. Heatmap of the water quality parameters highlighting hotspots near delta region. The horizontal line indicates river-like dominant conditions, the delta, and the lake .	33
Figure 15. Conceptual diagram comparing monsoon and post-monsoon hyperpycnal flows based on sensor data.....	33

LIST OF TABLES

Table 1. Parameters and corresponding sensors and sampling frequencies available in our study	5
Table 2. Grab sampling locations	10
Table 3. Calibration standards, reagents, and method detection limit (MDL) of analytes	13
Table 4. Transect length, lake elevation, and discharge values during field campaigns. Discharge values are contextualized with past records, showing high values in green and low values in red.....	25

1. JUSTIFICATION OF WORK PERFORMED

Wildfires, not long ago seen as occasional watershed disturbances that could be fiscally managed as non-recurrent disasters, have become repetitive and predictable catastrophes. New Mexico is frequently under severe or exceptional drought conditions and is particularly vulnerable to wildfires (Ball et al. 2021). The increased frequency and severity of wildfires in New Mexico causes overwhelming impacts to fluvial systems and vulnerable groups, such as Hispanic and Native American communities, which experience about 50% greater vulnerability to wildfires compared to other affected communities (Davies et al. 2018). To move us beyond the status quo of solely relying on the fortuitous monitoring of wildfire disturbances, we monitored the propagation of aquatic disturbances associated with the Hermit's Peak/Calf Canyon Fire along the Gallinas Creek – Pecos River network and into Santa Rosa Lake. For this, we created a rapid-response team (RRT) capable of deploying a multi-node sampling network to capture rapid changes in hydrology, water quality, and the transport and processing of nutrients team (Tunby 2022). Our RRT approach enabled us to study wildfire disturbances on demand, using standardized methods, and it was designed to overcome difficulties inherent in capturing post-fire wildfire disturbance propagation, that is, 1) it is difficult to predict when or where a wildfire will start, and 2) storm events mobilizing fire-byproducts (sediments, nutrients, and organic carbon stocks) yield rapid, abrupt changes in water quality that are difficult to capture with traditional sampling strategies.

The Hermit's Peak/Calf Canyon Fire is the largest and most catastrophic fire in New Mexico's recorded history (LeComte 2023). The Hermit's Peak Fire began on April 6, 2022, due to a prescribed burn on the Pecos – Las Vegas Ranger District of the Santa Fe National Forest, ~20 km (12 mi) northwest of Las Vegas, New Mexico. The Calf Canyon Fire started on April 19, 2022, due to a pile burn holdover from January 2022. The fires merged on April 23, 2022, and burned approximately 1383 km² (341,735 acres). The Burned Area Emergency Response (BAER) team classified about 324 km² (80,000 acres) as severely burned. Nearly 121 km² (30,000 acres) in the Gallinas and Tecolote Creek watersheds were burned. Gallinas Creek is the primary source of drinking water in Las Vegas, New Mexico, and supplies nearly 13,000 people. Gallinas Creek became contaminated with debris from the burned areas soon after the North American Monsoon System started to bring sustained increases in precipitation around June 15, 2022. Rain falling on burned areas during the Monsoon

consistently induced soil erosion, debris flows, and lateral flooding, all of which caused reduced water quality along Gallinas Creek and other streams within and downstream of the Hermit's Peak/Calf Canyon burn scar.

Since fire models predict the prevalence of wildfire and associated damage due to anthropogenic climate change and forest management practices (Adams 2013; Calkin, Thompson, and Finney 2015; North et al. 2015; Westerling et al. 2011; Abatzoglou and Williams 2016), there is a need to quantify the propagation of wildfire disturbances through fluvial networks to mitigate impacts to water quality and to protect ecosystem services. However, data on post-fire water quality propagation have only been fortuitously measured in a few study cases. The limited data available have revealed impacts over hundreds of kilometers (Reale et al. 2015; Dahm et al. 2015; Abram et al. 2003), affecting reservoirs and municipal water supply systems (Bladon et al. 2014).

Using the targeted, high-resolution water quality and meteorological data collected in this study, we address how far downstream water quality disturbances propagate after the Hermit's Peak/Calf Canyon wildfire, the role of seasonality in that propagation, and the impact of Santa Rosa Lake in mitigating further longitudinal propagation.

2. REVIEW OF METHODS USED

2.1. Rapid Response Team (RRT) monitoring with sensors

2.1.1. Equipment used

We deployed YSI EXO2 multiparameter water quality sondes at five sites within the Gallinas and Pecos watershed (Figure 1). The University of New Mexico's Center of Water and Environment (UNM CWE) maintains three of the sites within the Gallinas watershed located at Gallinas, NM (referred to as GFT), Montezuma, NM (GMZ), and Lourdes, NM (GL). The other two sonde sites are maintained by the U.S. Army Corp of Engineers (USACE) in collaboration with the University of New Mexico and are located on the Pecos River approximately 2 km upstream of Santa Rosa Lake (PSR) and 0.5 km downstream of Santa Rosa Lake (PBS). UNM CWE sonde sites were deployed on April 25, 2022, while the USACE sites were deployed in 2020. All sites, except for the GFT due to sensor damage, are currently being monitored and we plan to continue monitoring into 2023. All EXO 2 sondes measure water temperature, specific conductivity, dissolved oxygen, turbidity, and pH at 15-min intervals. On September 4, 2022, the dissolved oxygen sensor at PSR was damaged, and started producing negative values, and was subsequently excluded from the analysis. In addition, sondes maintained by UNM CWE measure fluorescent dissolved organic matter (fDOM) at 15-min intervals. All sondes were cleaned and calibrated at monthly intervals in accordance with USGS guidelines (Wagner et al. 2006).

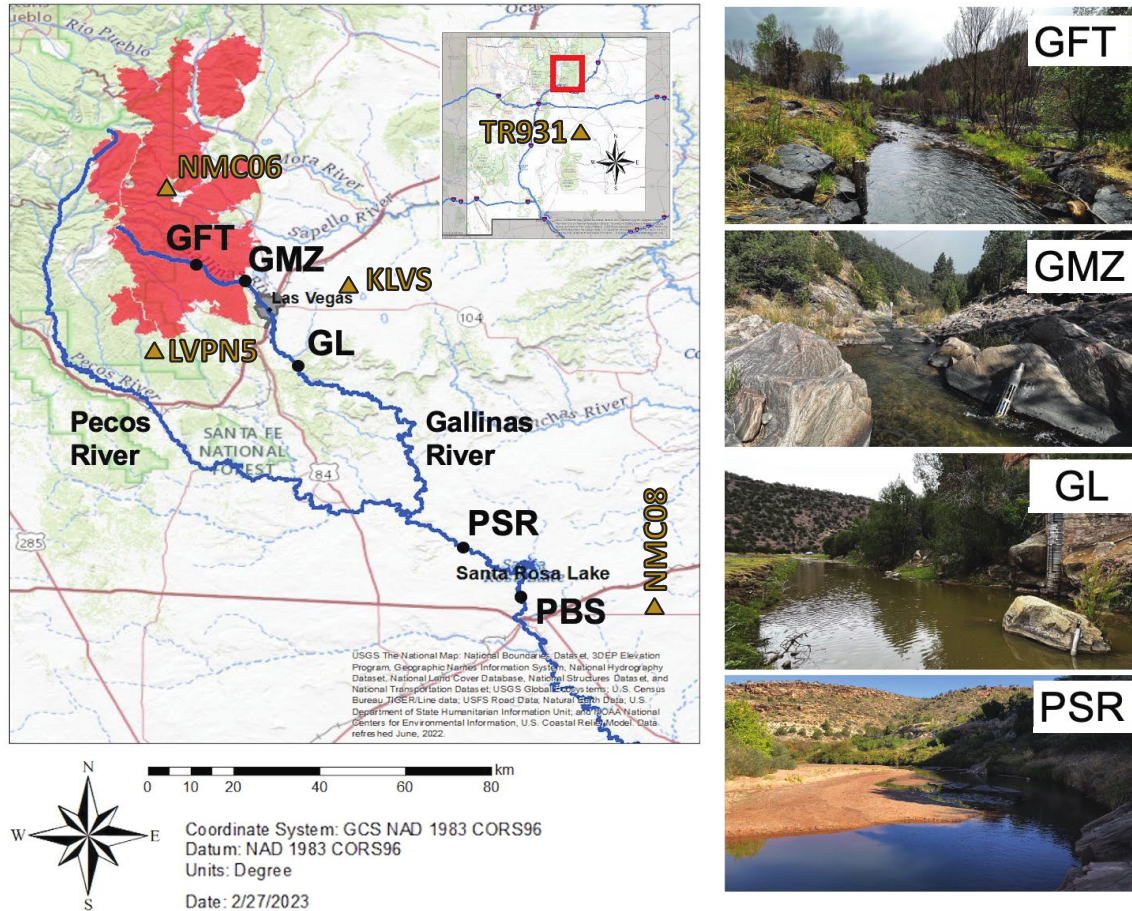


Figure 1. Site map of sensor deployment. Red highlighted region represents the burn boundary of the Hermit's Peak/Calf Canyon Fire.

Discharge and stage data were collected at 15-minute intervals by USGS stream gages 08380400, 08380500, 08382000, 08382650, and 08382830, and were collocated near sonde sites GFT, GMZ, GL, PSR, PBS, respectively. Meteorological data were exported from MesoWest with barometric pressure being measured at climate station KLVS, precipitation at stations LVPN5, KLVS, and GSCN5, and solar radiation at stations LVPN5, GSCN5, TR931 at 10-min intervals (Table 1). Precipitation and solar radiation time series from multiple sites were aggregated to a single time series by taking the weighted average on the proximity of a sonde site to the respective climate station. Differences between the sonde site's and KLVS's barometric pressure are accounted for by a factor of 160 Pascals per 15.4 m in elevation difference.

Table 1. Parameters and corresponding sensors and sampling frequencies available in our study.

Source	Parameter	Abbreviation	Units	Sites	Sampling Frequency (min)
USGS	Discharge	Discharge	m ³ s ⁻¹	GMZ, GL, PSR, PBS	15
	Stage	Stage	m	GFT, GMZ, GL, PSR, PBS	15
YSI EXO2	Dissolved oxygen	DO	ppm	GFT, GMZ, GL, PSR, PBS	15
	Specific conductivity	Sp Cond	uS cm ⁻¹	GFT, GMZ, GL, PSR, PBS	15
	Water temperature	Water Temp	°C	GFT, GMZ, GL, PSR, PBS	15
	Turbidity	Turbidity	FNU	GFT, GMZ, GL, PSR, PBS	15
	pH	pH	-	GFT, GMZ, GL, PSR, PBS	15
	Fluorescent dissolved organic matter	fDOM	QSU	GFT, GMZ, GL	15
MesoWest	Barometric pressure	Baro Press	mmHg	KLVS	10
	Solar radiation	PAR	μmol m ⁻² s ⁻¹	LVPN5, TR931, NMC08, NMC06	10
	Precipitation	Precip	mm	LVPN5, TR931, NMC08, NMC06	10

2.1.2. Raw data conversions

fDOM was corrected for changes in water temperature and turbidity using the following equations (Regier et al. 2020; Downing et al. 2012):

$$fDOM_{temp} = \frac{fDOM}{1 + \rho(W_T - T_1)} \quad (1)$$

$$fDOM_{cor} = \frac{fDOM_{temp}}{a + b * exp(c*turb)} \quad (2)$$

where $fDOM_{temp}$ is the temperature corrected fDOM concentration (QSU; Quinine Sulfate Units); fDOM is the uncorrected fDOM concentration (QSU); ρ is temperature-specific fluorescence coefficient of $-7.545 \times 10^{-3} \text{ } ^\circ\text{C}^{-1}$; W_T is the water temperature ($^\circ\text{C}$); T_1 is the lab temperature of $22 \text{ } ^\circ\text{C}$ when fDOM was calibrated; $fDOM_{cor}$ is the temperature and turbidity corrected fDOM concentration (QSU); *turb* is the water turbidity (FNU; Formazin Nephelometric Units); *a*, *b*, and *c* are turbidity correction coefficients of 0.38901, 0.72842, and

-0.00618 when turbidity is less than 600 FNU, or 0.17573, 0.25597, and -0.00038 when turbidity is greater than 600 FNU.

Photosynthetically active radiation (PAR) was derived by multiplying total solar radiation by a factor of 2.04 (Meek et al. 1984). Average stream depth was derived by dividing the measured water column area by its width from 2000 to 2022 USGS discharge field measurements taken at each USGS stream gage. Due to USGS stream gage 08380400 not having any historical field measurements, a relationship was developed between measured sonde depth and non-contact radar gage height to establish an average depth. Lastly, during periods prior to the deployment of non-contact radar, USGS stream gage 08380400 gage height was estimated using a two-hour lagged relationship between USGS 08380500 and 08380400 gage heights during periods when both gages were operational. The following relationships were used to calculate the average depth at GFT, GMZ, GFT, and PSR, respectively:

$$Depth_{GFT} = 0.660 * Stage_{08380400} + 1.30 \quad (3),$$

$$Depth_{GMZ} = 0.351 * Q_{08380500}^{0.308} \quad (4),$$

$$Depth_{GL} = 0.317 * Q_{08382000}^{0.234} \quad (5),$$

$$Depth_{PSR} = 0.1822 * Q_{08382650}^{0.368} \quad (6),$$

$$Depth_{PBS} = 0.354 * Q_{08382830}^{0.326} \quad (7),$$

where $Depth_{site}$ is the estimated average depth of the water column (m), $Stage$ is the recorded USGS gage height (m), and Q is the recorded discharge at the USGS stream gage site (m^3s^{-1}).

2.1.3. Data quality control and assurance

Raw and converted data were processed for outliers and sensor drift with Aquarius Timeseries 21.1. Erroneous outliers were eliminated by using a moving average filter targeting points deviating more than 20% from a two-hour moving window. We corrected for sensor drift and biofouling by comparing pre- and post-cleaning and calibration values. We applied a linear correction from the date of the previous maintenance. Lastly, a final visual inspection of data quality was performed prior to any statistical analysis.

2.1.4. Data Organization, Metabolic Modeling, and Statistical Methods

2.1.4.1. Periods of analysis

We separated the sonde time series data into three periods: pre-monsoon for values measured before June 26, 2022, monsoon for values measured from June 26 to September 14, 2022, and post-monsoon for values measured after September 14, 2022. MATLAB's *ischange* function was used on discharge data observed at USGS stream gage 08380500 to determine significant changes in the discharge's mean trend, and the first and the last inflection points in trend change were used to delineate temporal periods. MATLAB's *ischange* function determines points of significant change in a time series mean trend by iteratively minimizing the sum of the following cost function:

$$C(A_1) + C(A_2) + C(A_k) + k\tau < C(A) \quad (8)$$

$$C(A_k) = n * var(A_k) \quad (9)$$

where A is the timeseries being analyzed for abrupt changes; k is the maximum number of change points set to 10, τ is a threshold limit determined by k ; and n is the number of data points in timeseries A_k .

2.1.4.2. Stream Metabolism

We estimated daily averages of stream metabolism using the USGS Stream Metabolizer model (Appling et al. 2018; Odum 1956), which uses a one-station model based on the open-channel metabolism approach (Equations 10-12), which utilizes inverse Bayesian modeling to estimate gross primary production (GPP), ecosystem respiration (ER), and re-aeration coefficients (K_{600}). GPP quantifies DO production and organic carbon production from phototrophic communities, ER quantifies DO losses and inorganic carbon production due to autotrophic and heterotrophic respiration, and K_{600} is a standardized oxygen gas exchange rate coefficient between the water column and the atmosphere. The modeling equations used in Stream Metabolizer are:

$$\frac{dDO_t}{dt} = \frac{1}{Z_t} \left(\frac{GPP(t_1 - t_0) * PPF D_t}{\int_{u=t_0}^{t_1} PPF D_u du} + ER \right) + \frac{K_{600}(DO_{sat,t} - DO_{mod,t})}{\sqrt{\frac{S_A - S_B T_t + S_C T_t^2 + S_D T_t^3}{600}}} \quad (10)$$

$$DO_{mod,t} = DO_{mod,t-\Delta t} + \int_{u=t-\Delta t}^t \left(\frac{dDO_{mod,u}}{du} + \varepsilon_{proc,u} \right) du \quad (11)$$

$$DO_{obs,t} = DO_{mod,t} + \varepsilon_{obs,t} \quad (12)$$

where DO_t is the observed dissolved oxygen (mg L^{-1}) at time t ; $DO_{sat,t}$ is the hypothetical saturated dissolved oxygen concentration (mg L^{-1}); $DO_{mod,t}$ is the modeled dissolved oxygen concentration (mg L^{-1}); ε_{obs} and ε_{proc} are the observation and processes errors; t_0 and t_1 are the beginning and end of the day (d); Z_t is stage (m); $PPFD_t$ is solar radiation as PAR ($\mu\text{mol m}^{-2} \text{d}^{-1}$); T_t is the water temperature ($^{\circ}\text{C}$); $S_{A,B,C,D}$ are dimensionless Schmidt coefficients (-); GPP is the daily average areal rate of gross primary production ($gO_2 m^{-2} d^{-1}$); ER is the daily average areal rate of ecosystem respiration ($gO_2 m^{-2} d^{-1}$); and K_{600} is the standardized gas exchange rate coefficient (d^{-1}).

2.1.4.3. Exceedance Probability

Exceedance probabilities of maximum daily discharge were calculated from available recorded discharge values at USGS stream gages 08380500, 08382000, and 08382650. Discharge records used to calculate exceedance probabilities extended from October 1, 1990, to November 8, 2022, for stream gages 08380500 and 08382650, and from March 13, 2006, to November 8, 2022, for stream gage 08382000. First, the 15-minute discharge measurements were aggregated by the maximum daily value observed during a single day. The maximum daily discharge values were sorted and ranked from highest to lowest, with the highest discharge value ranked 1 and the smallest ranked the total number of observations. Exceedance probability could then be calculated for each daily maximum discharge value (Kinchon 1959):

$$P_{exceedance} = 100 * \frac{M}{(n + 1)} \quad (13)$$

where $P_{exceedance}$ is the calculated exceedance probability for a given daily maximum discharge, M is the numeric rank for given daily discharge, and n is the total number of daily discharge observations.

2.1.4.4. Principal component analysis

We examined the relationships between parameters using a principal component analysis (PCA) conducted using Matlab's *pca* function. The first two principal components were used for statistical analysis since each site's first two components explained approximately 60% of the total variance. The first two principal components were plotted in a biplot to determine relationships between parameters visually. Parameters aligned in the same direction are positively correlated, those in opposite directions are negatively correlated, and those orthogonal are uncorrelated (Jolliffe and Cadima 2016). We calculated daily averages for aquatic and meteorological parameters to be able to include daily stream metabolism estimates. Lastly, we standardized each parameter's daily average by centering its mean at zero and scaling by its standard deviation to make parameters with varying magnitudes and units comparable:

$$S_X = \frac{X - \mu_X}{\sigma_X} \quad (14)$$

where S_X is the standardized parameter X (-), and μ_X and σ_X are the mean and standard deviation of parameter X .

2.2 RRT Monitoring with grab sampling

2.2.1 Sampling locations

Using grab sampling, we monitored water quality parameters from 16 sites along a fluvial network extending 178 km from near the fire perimeter to Santa Rosa Lake. In 4 of those 16 grab sampling sites, we had YSI EXO 2 water quality sondes measuring water quality parameters every 15 min. The grab sampling sites are listed in Table 2 and shown in Figure 2. Grab water samples were collected at different sites before the monsoon period, during the monsoon period, and after the monsoon period, primarily in response to storm events. Grab water samples were collected from sensor sites during maintenance visits beginning in April 2022. The sensor maintenance was scheduled every two to three weeks before and during the monsoon period, and once a month after the monsoon period. After filtering the samples using 0.45-micron pore-size membranes, the samples were inserted into 20 ml vials, and were stored in a cooler with ice during field hours and in a freezer upon return to the UNM laboratory until the samples were analyzed.

Table 2. Grab sampling locations.

Site No.	Site ID	Sampling Location	Distance (km)
1	GEV	Gallinas EV Long	0.0
2	GFT	Gallinas Fire Station at El Porvenir	6.8
3	GMZ	Gallinas near Montezuma	12.1
4	GD	Gallinas at skating pond outlet (Dam)	15.1
5	GHS	Gallinas near Hot Springs	16.1
6	GB	Gallinas at Bridge Near United World	16.9
7	GC	Gallinas at Downtown (City)	26.1
8	GI25	Gallinas near I-25	28.9
9	GL	Gallinas near Lourdes	48.5
10	GCL	Gallinas near Colonias	125.8
11	PSR	Pecos River near Santa Rosa	159.8
12	D1	Delta near Santa Rosa Lake	171.8
13	Old D1	Old Delta near Santa Rosa Lake	174.6
14	SR-1	Santa Rosa Lake	175.2
15	SR-2	Santa Rosa Lake	176.5
16	SR-3	Santa Rosa Lake	178.3

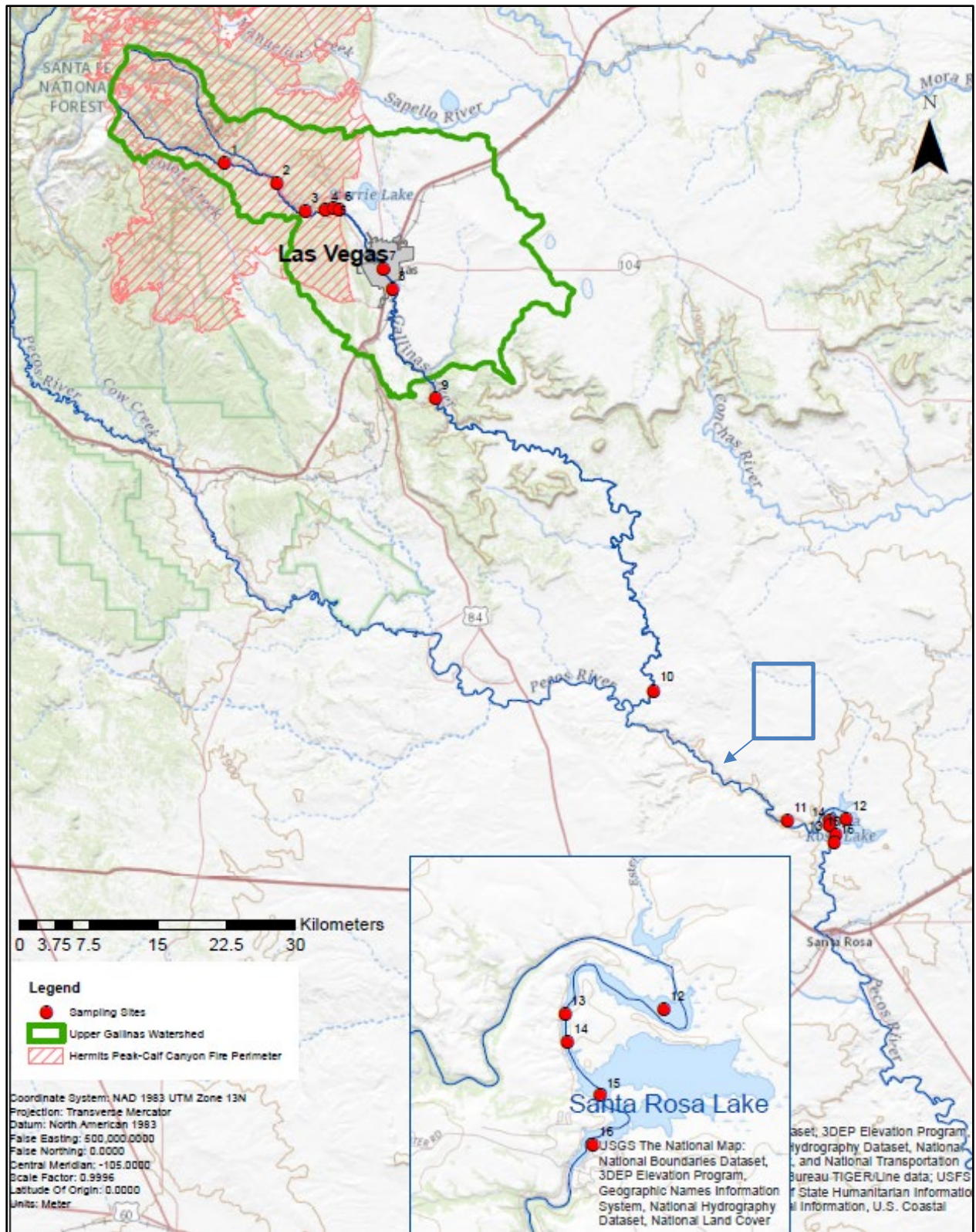


Figure 2. Grab sampling locations.

2.2.2 Grab Sample Analysis

Wildfires may impact several water quality indicators including various inorganic and organic constituents such as nitrate (NO_3^-), nitrite (NO_2^-), ammonium (NH_4^+), sulphate (SO_4^{2-}), phosphate (PO_4^{3-}), organic carbon, and other nutrient loadings (Smith et al. 2011). For the current study, the concentration of nitrate, nitrite, total oxidized nitrogen (TON), ammonium, sulphate, and phosphate have been analyzed using a Thermo Fisher Scientific Gallery Discrete Analyzer. For sulphate, ammonium, and phosphate, the instrument uses the colorimetric method. For TON, nitrite, and nitrate, the instrument uses the colorimetric hydrazine method. Colorimetric analysis is referred to as a method for determining the concentration of chemical species or chemical compounds with the aid of a color reagent (Thermo Fisher Scientific Inc. 2015).

For determining the concentration of ammonium ion, the instrument measures the absorbance of a blue compound spectrophotometrically at a wavelength of 660 nm, which is later related to the ammonia concentration via calibration. The blue compound is formed when ammonia reacts with hypochlorite ions and salicylate ions present in the reagents. For determining the concentration of phosphate ion, the instrument measures the absorbance of a blue heteropoly compound spectrophotometrically at a wavelength of 880 nm, which is later related to the phosphate concentration via calibration. The blue heteropoly compound is formed when the orthophosphate ion reacts with ammonium molybdate, and antimony potassium tartrate present in the reagents. Likewise, the instrument determines the sulphate ion by measuring the turbidity that results from the precipitation of the sulphate ions in a strong acid medium with barium chloride. The turbidity is measured photometrically at 405 nm and compared with the calibration curve. For determining the TON, the absorbance of a pink compound is measured at a wavelength of 540 nm, which is related to TON concentration via calibration. The pink compound is formed when the nitrate is reduced to nitrite by hydrazine under an alkaline environment, which later reacts with sulphanilamide and N-1-naphthylethylenediamine dihydrochloride present in the reagents under acidic conditions. The nitrate concentration is calculated by the instrument automatically by subtracting the measured values of nitrite from TON (Table 3).

Table 3. Calibration standards, reagents, and method detection limit (MDL) of analytes.

Analyte	Reagents	Calibration Standards (mg/l)	Calibration Verification Standards (mg/l)	Theoretical MDL in mg/l ($3.14 \times SD$ (blank sample, $n=7$))
Ammonium Low	Ammonia R1, Ammonia R2	0, 1	0.1	0.0005 as Nitrogen(N)
Phosphate Low	Phosphate R1, Phosphate R2	0, 1	0.1	0.0004 as Phosphorous(P)
Phosphate High	Phosphate R1, Phosphate R2	10	1.1	N/A
Sulphate Low	Sulphate R1	0, 1000	10	0.26
Sulphate High	Sulphate R1	1000	40	N/A
TON low (nitrate + nitrite) and nitrate by calculation	TON R1, TON R2, TON R3	0, 10	1	0.0006 as Nitrogen(N)
Nitrite	TON R3	0, 10	0.4	0.0004 as Nitrogen(N)

Thermo Fisher Scientific Inc., (2018).

2.2.3 Quality Control

Prior to the analysis of the sample, the calibration of the instrument is performed for each species, that is, total oxidized nitrogen (TON), nitrite (NO_2^-), ammonium (NH_4^+), sulphate (SO_4^{2-}), and phosphate (PO_4^{3-}) using the calibration solution of the respective species. After the calibration test, the instrument generates the calibration curve along with the coefficient of determination (R^2), which is verified and accepted manually if the R^2 values are closer to 1 (Figure 3). Then, the concentrations for calibration verification standards (CCVs) are tested for each species. These calibration solutions and calibration verification standards (CCVs) are prepared using a stock solution of each compound by adopting a dilution method. The CCVs are run immediately after the calibration is accepted. The results from the calibration curve and tests on CCV are accepted if the measured values are within 90 to 110% of the true values. Along with the CCVs, the initial calibration blanks are also run to evaluate the background concentration of each constituent for each analytical procedure. Grab samples are tested only

after the values of CCVs are verified and accepted. If the values of CCVs do not pass, necessary corrective measures are applied. After every ten samples and at the end of the test, the mid-point calibration verification test is performed to verify the concentration of CCVs and calibration blanks.

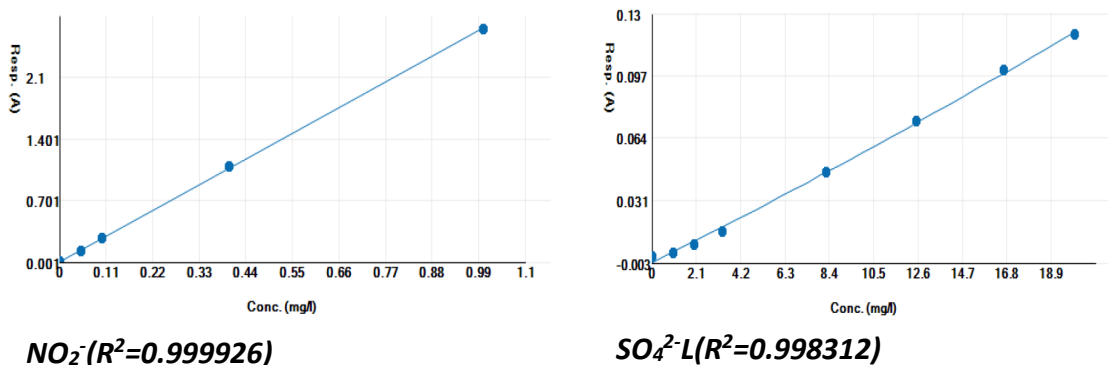


Figure 3. Example of calibration curves from the test methods of different species.

Grab sample data were categorized into the same three periods as the sonde data, that is, pre-monsoon (before June 26), monsoon (June 26 to September 14), and post-monsoon (after September 14).

2.3 RRT with The Navigator

In collaboration with the USACE Albuquerque District, our RRT crew conducted Lagrangian water quality monitoring (i.e., as the flow goes) using high-resolution sensors in Santa Rosa Lake. Between July 15, 2022, and October 12, 2022. We monitored the spatiotemporal variability of physical, chemical, and biological parameters measured at the lake's surface to characterize post-fire disturbances and their propagation through fluvial networks into reservoirs.

Most Lagrangian monitoring was based on data from our team's Navigator, which is a miniature boat made of fiberglass, instrumented with a GPS tracker (to monitor space-time variations and to allow sensor recovery), a thrust and rudder system to follow a preplanned GPS waypoint, and a Raspberry Pi microcontroller coupled to multiparameter sonde monitors for the temperature (temp), optical dissolved oxygen (DO), turbidity (turb), and pH and conductivity (Sp Cond). The Navigator features real-time data transmission through cellular service, enabling real-time tracking and easy retrieval when the survey is completed. To avoid data losses from

any potential malfunctioning of The Navigator, we also used a kayak carrying a multiparameter YSI EXO2 sonde and a GPS (Figure 4).

We monitored a longitudinal profile near the confluence of the Pecos River and Santa Rosa Lake to explore water quality changes associated with wildfire disturbance propagation through fluvial networks. Gallinas Creek, which was directly impacted by the wildfire, drains into the Pecos River ~40 km upstream of Santa Rosa Lake. We focused on determining how the transition from the Pecos River (a lotic system) into Santa Rosa Lake (a lentic system) impacts water quality parameters in space and time. Over the four months of this study, we carried four repetitions of Lagrangian monitoring following transects of 30.5 km.



Figure 4. The Navigator monitoring water quality in Santa Rosa Lake (left), and the kayak with the multiparameter sonde monitoring the Pecos River (right).

3. DISCUSSION OF RESULTS AND THEIR SIGNIFICANCE

3.1. RRT monitoring with sensors

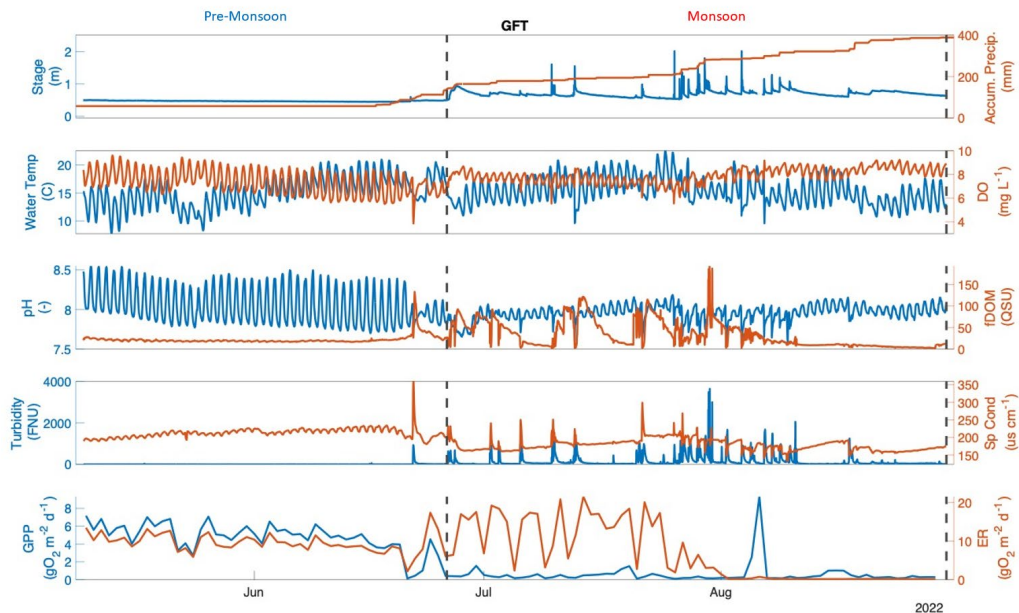
3.1.1. Pre-Monsoon period

No significant precipitation events occurred during the pre-monsoon season, with a total cumulative precipitation of 54.6 mm near GFT. The lack of pre-monsoon precipitation resulted in discharge being at its lowest during the study period, with average discharges ranging from 0.05 to 0.17 m^3s^{-1} across the sonde sites (Figure 5).

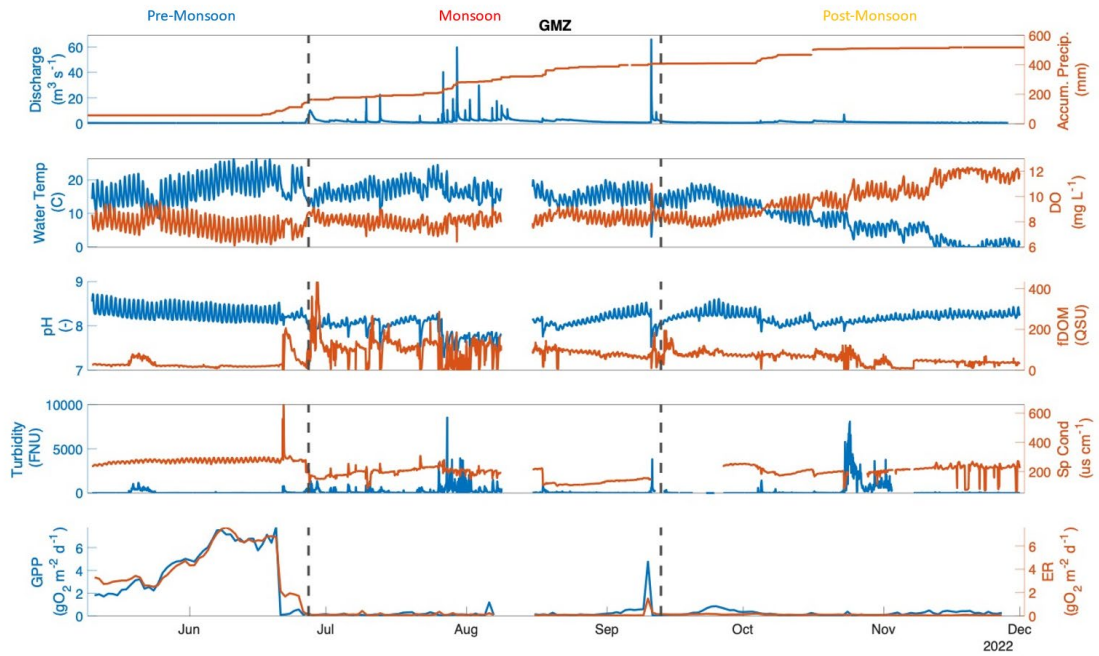
Turbidity and fDOM were at their lowest values at sonde sites upstream of Santa Rosa Lake, with averages ranging from 5.89 to 62.5 FNU and 21.7 to 31.7 QSU. The PBS site had its highest turbidity during the study period with an average of 16.7 FNU. There was a significant increase in specific conductivity from the upper study reaches to the lower study reaches with a difference of 2300 uS/cm between GFT and PSR pre-monsoon averages.

Gross primary production site averages ranged from 0.66 to 9.83 $gO_2 m^{-2} d^{-1}$ during the pre-monsoon season, with the highest values occurring at GL. Ecosystem respiration mirrored gross primary production through the monitoring sites, with GL having the highest pre-monsoon average of 14.9 $gO_2 m^{-2} d^{-1}$ (Figure 5).

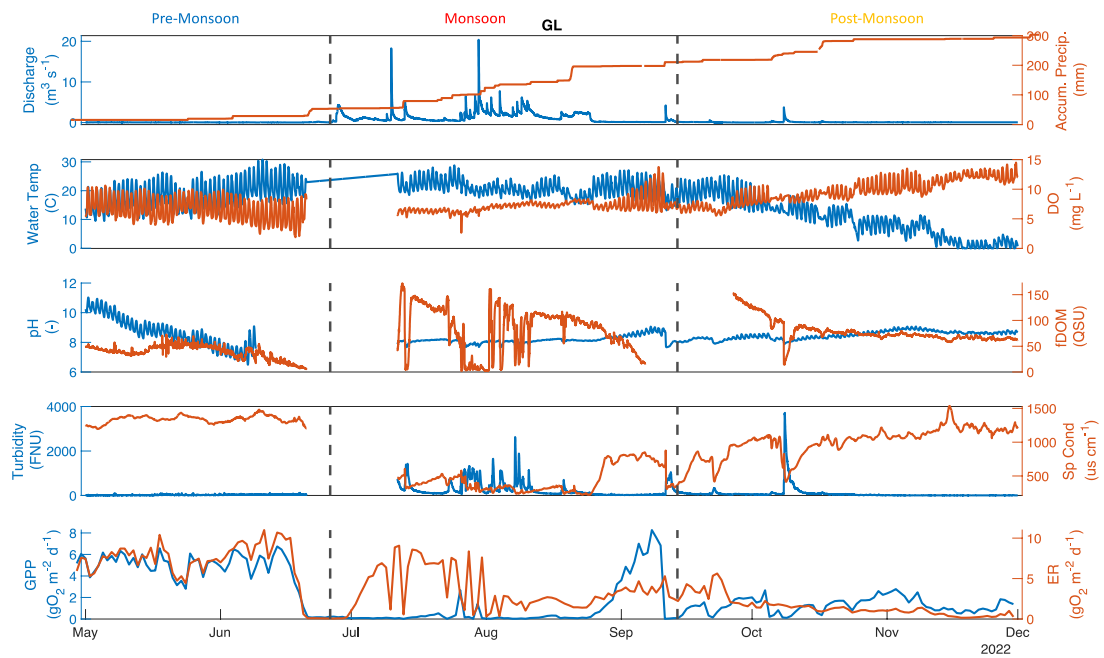
A) GFT monitoring site: upstream of Santa Rosa Lake



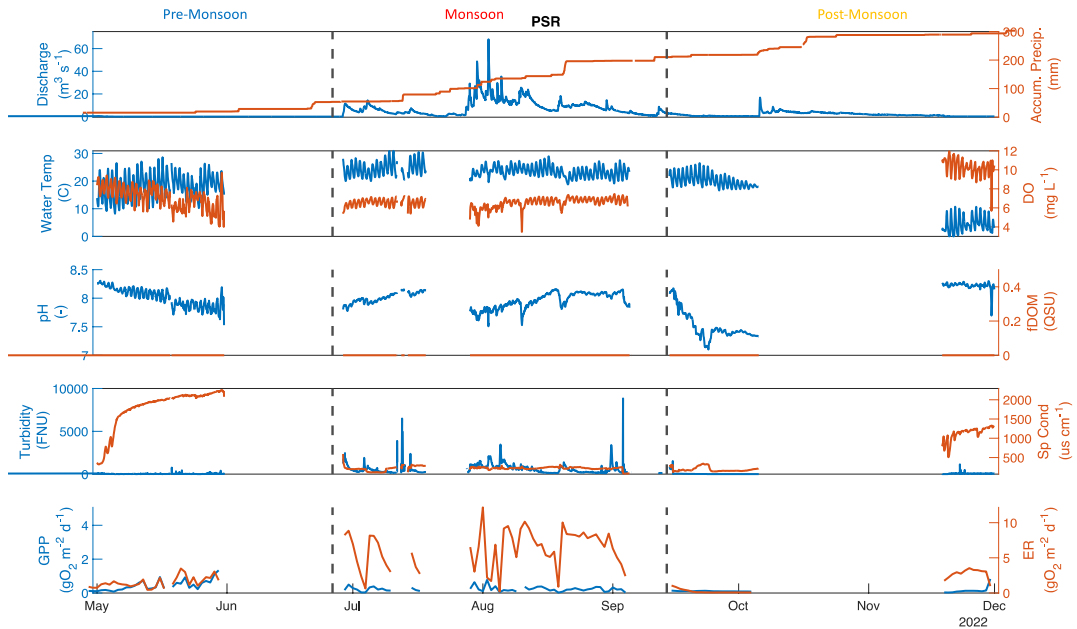
B) GMZ monitoring site: upstream of Santa Rosa Lake



C) GL monitoring site: upstream of Santa Rosa Lake



D) PSR monitoring site: upstream of Santa Rosa Lake



E) PBS monitoring site: downstream of Santa Rosa Lake

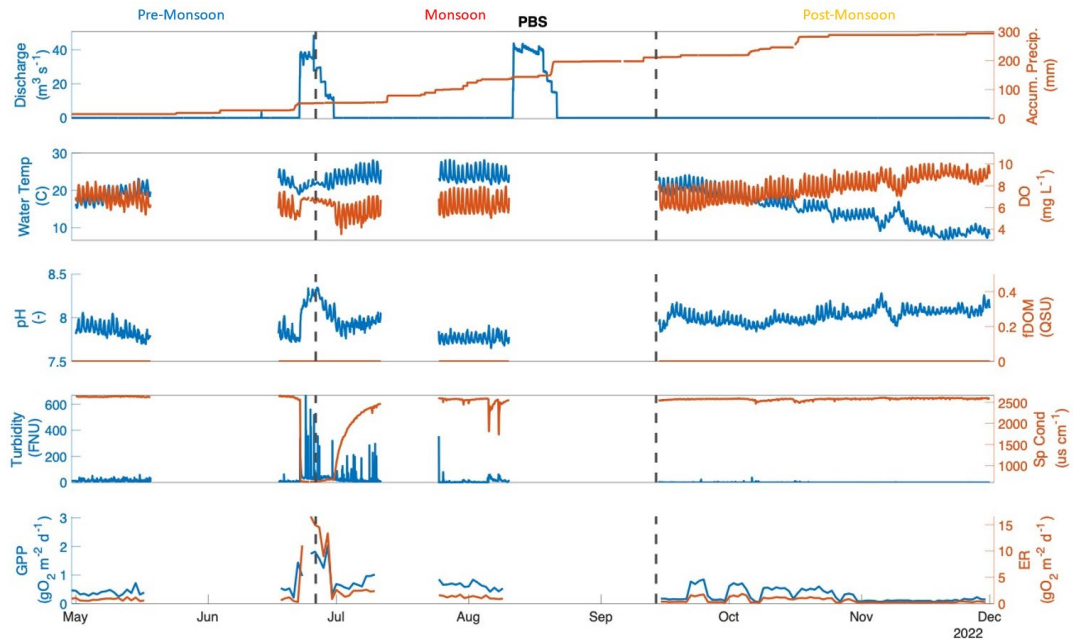


Figure 5. QA/QC timeseries data from EXO2 water quality sondes and weighted average precipitation from nearby climate stations. Data collected at A) Gallinas Creek near Gallinas, B) Gallinas Creek near Montezuma, C) Gallinas Creek near Lourdes, and Pecos River D) upstream and E) downstream of Santa Rosa Lake.

3.1.2. Monsoon period

The monsoon period received significant precipitation, with a total increase of 287 mm at GFT and 159.3 mm at PSR. The resulting monsoon precipitation increased discharge at all sites, with average discharges ranging from 1.3 to 7.8 m³s⁻¹.

Turbidity and fDOM increased at the monitoring sites upstream of Santa Rosa Lake during the monsoon season, reaching maximum site averages of 496 FNU and 97.8 QSU at PSR and GMZ, respectively. There was a reduction in turbidity at the PSR site during the monsoon season with an average value of 13.3 FNU. There was a significant reduction in specific conductivity at the monitoring sites, with the largest reduction occurring at PSR of 1655 uS/cm (Figure 6). Diel cycling of pH and dissolved oxygen was attenuated at the monitoring sites upstream of Santa Rosa Lake during the monsoon period. For example, at the GMZ site, pre-monsoon pH and dissolved oxygen diel deltas of 0.5 and 2.2 ppm declined to deltas of 0.1 and 0.9 ppm during the monsoon (Figure 5).

GPP at monitoring sites upstream of Santa Rosa Lake experienced a significant reduction, with average values ranging from 0.404 $gO_2 m^{-2} d^{-1}$ at PSR to 3.21 $gO_2 m^{-2} d^{-1}$ at GL. There was a reduction in ER at all monitoring sites except for PSR and PBS, which experienced an average increase of 3.65 and 0.201 $gO_2 m^{-2} d^{-1}$ during the monsoon period. The most significant reduction in ecosystem respiration occurred at GMZ, which had a pre-monsoon average of 6.11 $gO_2 m^{-2} d^{-1}$ that declined to a monsoon average of 0.196 $gO_2 m^{-2} d^{-1}$ (Figure 6).

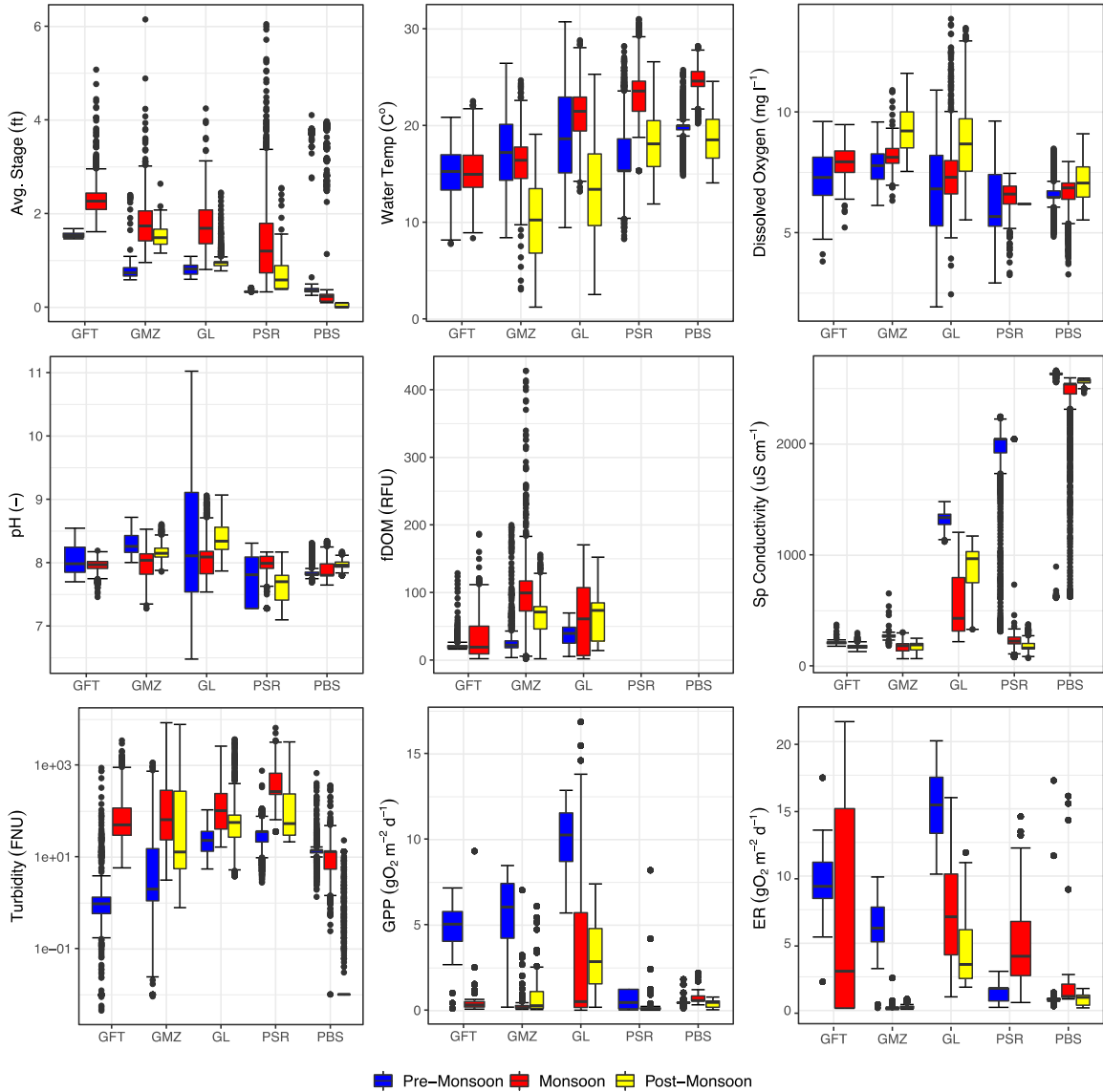


Figure 6. Boxplots of QA/QC data from water quality sondes at each site from April 26, 2022, through November 8, 2022.

3.1.3. Post-Monsoon period

The post-monsoon period experienced two precipitation events on October 6 and October 16, 2022, that produced 56.4 and 38.1 mm, respectively. The resulting precipitation events momentarily increased discharge from October 6 to November 2, 2022. Concurrently with the 28-day increase in discharge, turbidity also increased producing the highest observed value of 3680 FNU at GL (Figure 5).

At all monitoring sites, specific conductivity remained less than in the pre-monsoon period, while fDOM remained higher than in the pre-monsoon period (Figure 3). Diel cycling of pH and dissolved oxygen remained attenuated at monitoring sites upstream of Santa Rosa Lake during the post-monsoon period (Figure 5).

GPP at GMZ and GL increased during the post-monsoon period as compared to the monsoon season with averages of $1.04 \text{ gO}_2 \text{ m}^{-2} \text{ d}^{-1}$ and $3.16 \text{ gO}_2 \text{ m}^{-2} \text{ d}^{-1}$, respectively. GPP at PBS experienced little change from the monsoon season, with an average difference of $0.300 \text{ gO}_2 \text{ m}^{-2} \text{ d}^{-1}$. ER at GMZ maintained an average of $0.246 \text{ gO}_2 \text{ m}^{-2} \text{ d}^{-1}$, while ER at GL and PBS decreased to an average of 4.60 and $0.835 \text{ gO}_2 \text{ m}^{-2} \text{ d}^{-1}$. Due to sensor damage, GPP and ER could not be estimated at the GFT and PSR sites during the post-monsoon period (Figure 6).

3.2. RRT monitoring with grab sampling

At most of the sampling sites, the concentration of ammonium was high during the monsoon, medium in the post-monsoon, and low in the pre-monsoon stage (Figure 7). However, at Gallinas near the skating pond outlet (GD), the concentration of ammonium in the pre-monsoon period was the highest of all values recorded. Since the sampling location was near a dam, the elevated concentration of ammonium could be due to the lack of turbulence and mixing, which decrease the volatilization of ammonia and increase its concentration. The high concentration of ammonium during a monsoon is likely due to the release of debris flow from the burn scar area.

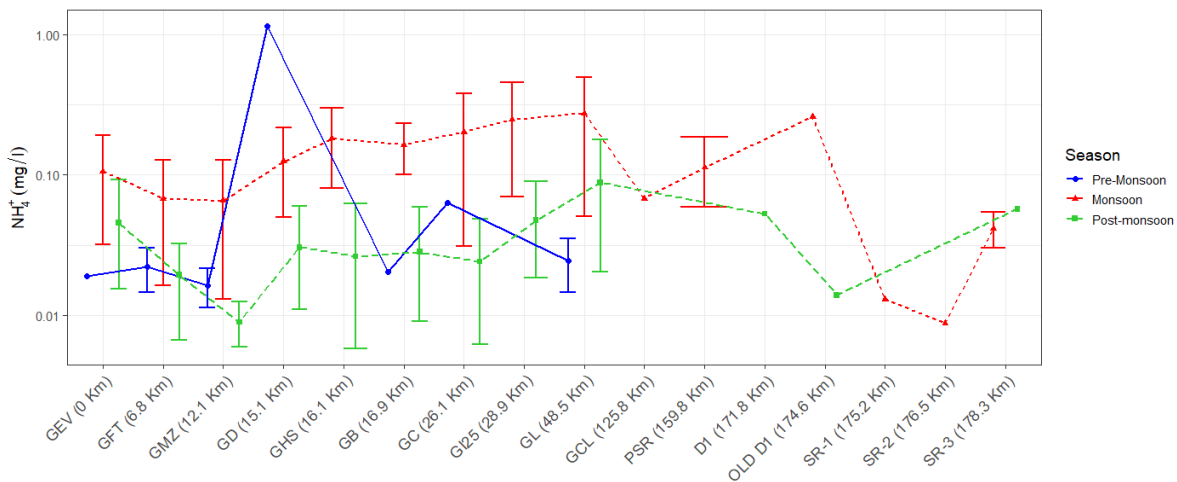


Figure 7. Concentrations of ammonium from Gallinas Creek to Santa Rosa Lake.

We observed a similar trend in the concentrations of phosphate compared to ammonium. At most of the sampling sites, the concentrations of phosphate were higher during the monsoon period, followed by post-monsoon (Figure 8). Although the concentration of phosphate has decreased post-monsoon, the values remain higher compared to pre-monsoon.

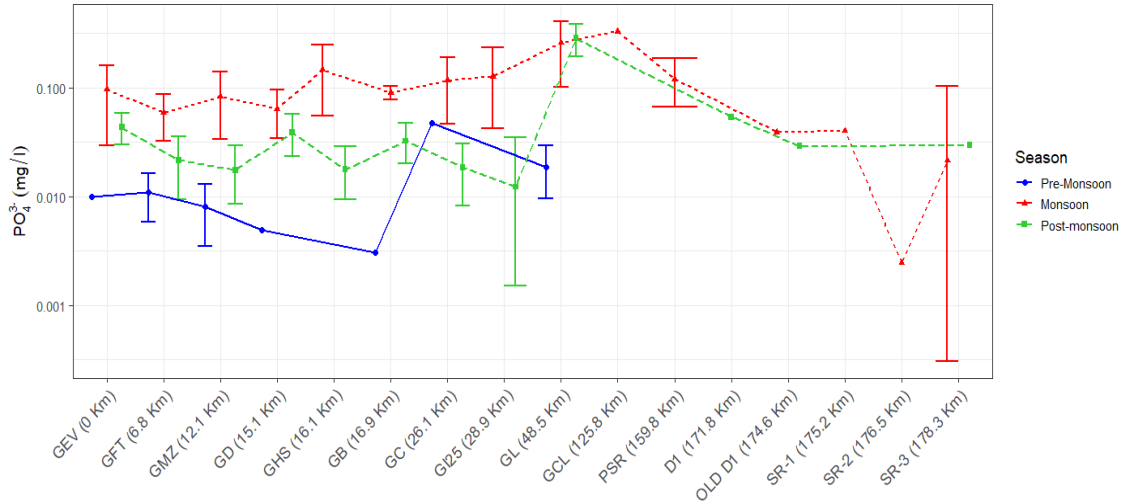


Figure 8. Concentrations of phosphate from Gallinas Creek to Santa Rosa Lake.

Most of the sampling sites within the fire perimeter (from GEV to GMZ) have elevated concentrations of sulphate during the monsoon and post-monsoon periods, compared to the pre-monsoon period (Figure 9). However, this trend shifts further downstream with concentrations being higher during the pre-monsoon period. Anthropogenic sources of contamination could be the possible reason for the high concentration of sulphate before the monsoon season, which were later diluted with the higher flows during the monsoon and post-monsoon periods. Similarly, near Gallinas Lourdes (GL), the possible reason for the high concentration of sulphate is the decomposition and combustion of organic matter, as there are cattle ranches near the river.

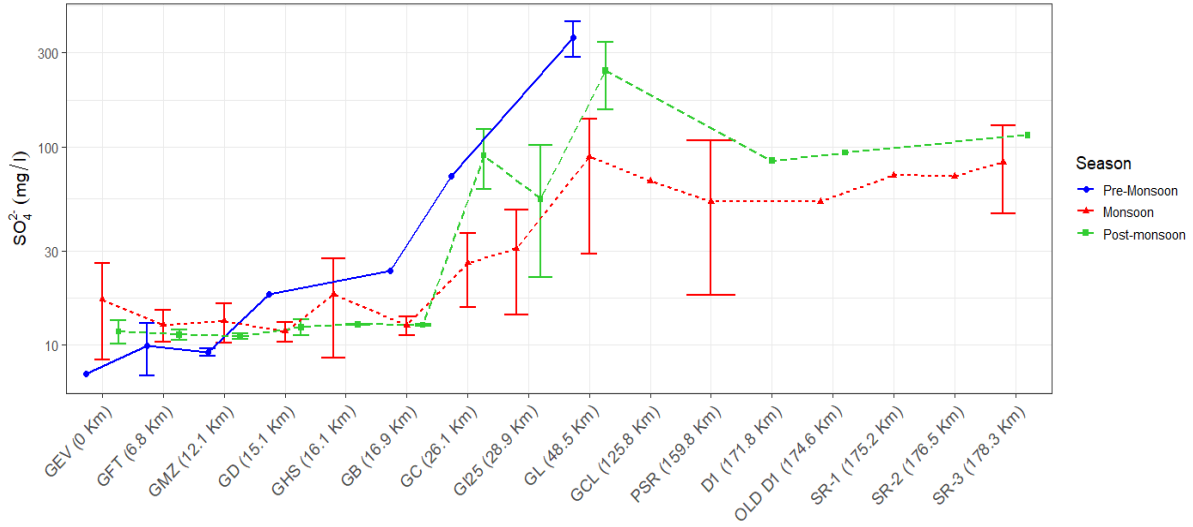
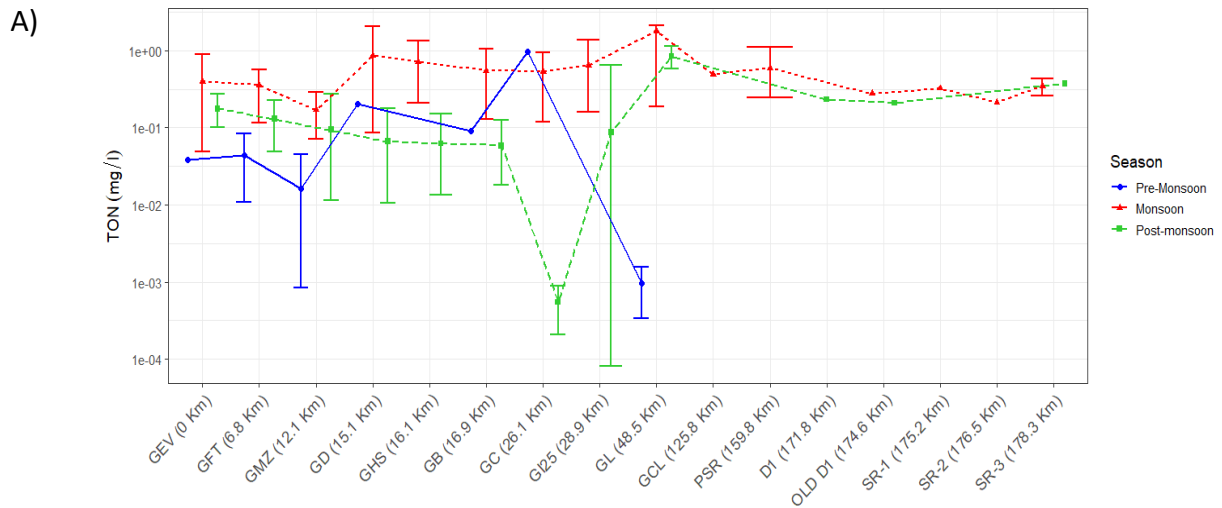


Figure 9. Concentrations of sulphate from Gallinas Creek to Santa Rosa Lake.

At most of the sampling locations, the concentrations of TON, nitrate, and nitrite were higher during the monsoon period. However, the concentration of nitrogen species was higher before the monsoon in the Gallinas Creek near the city of Las Vegas (GC). This could be due to various anthropogenic sources of contamination such as seepage from fertilized agricultural lands, municipal wastes, dumps, septic tanks, private sewage disposal systems, and so on.



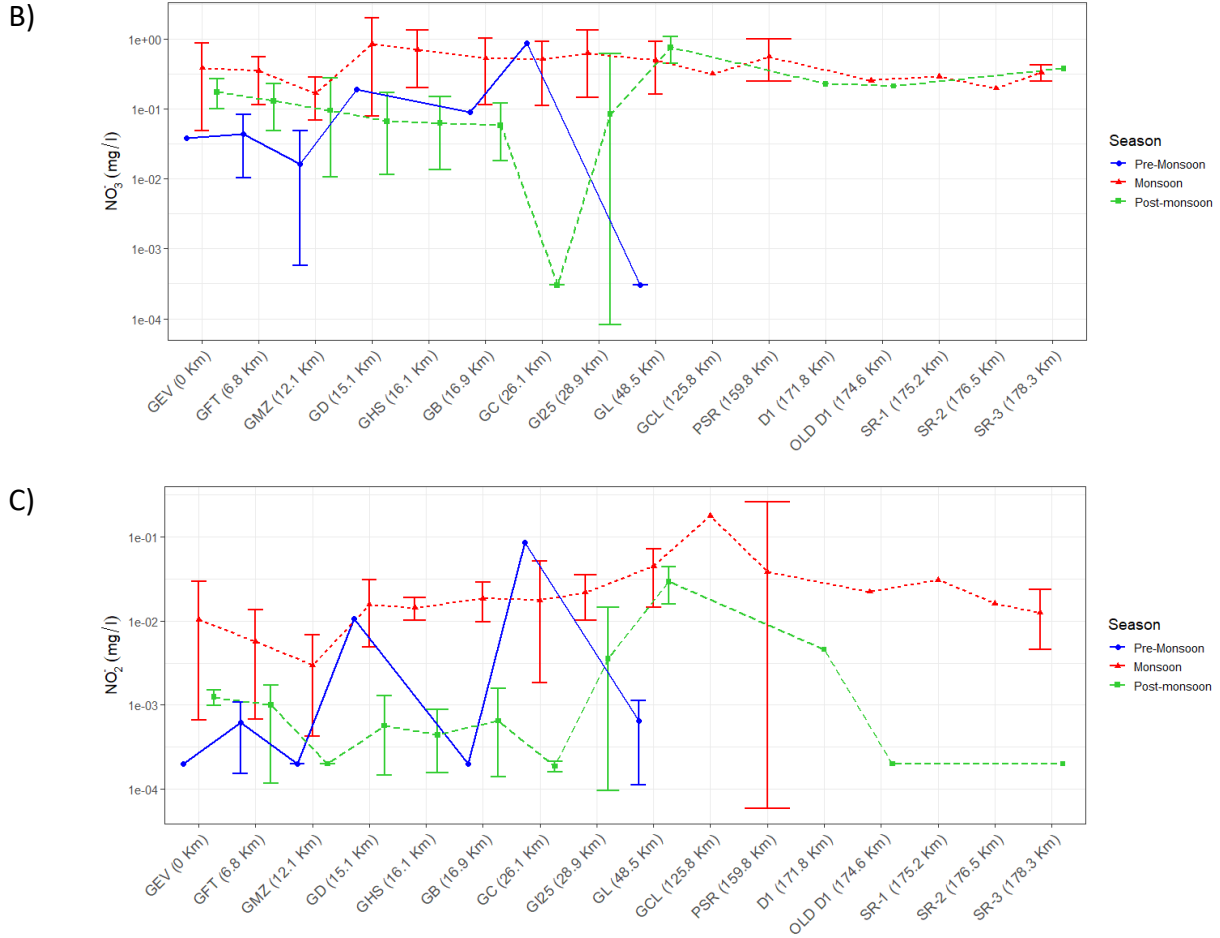


Figure 10. Concentrations of A) TON, B) nitrate, and C) nitrite from Gallinas Creek to Santa Rosa Lake.

3.2.1. RRT monitoring with The Navigator

The Lagrangian monitoring campaigns began in the morning and ended in the afternoon. After the first campaign, we avoided a reach consisting of rapids and a waterfall due to safety concerns. At the time of sampling, discharges in the Pecos River above Santa Rosa Lake (USGS gage 08382650) were above median historical values from 1977-2022 (Table 4). These higher discharge values were due to post-wildfire runoffs and the historically high monsoon precipitation falling in 2022. Similar trends were observed for Gallinas Creek near Colonias, NM (USGS gage 08382500).

Table 4. Transect length, lake elevation, and discharge values during field campaigns. Discharge values are contextualized with past records, showing high values in green and low values in red.

Date	Transect length	Lake elevation	Pecos River discharge 08382650	Comparable median Pecos River discharge (1977-2022)	Gallinas Creek discharge 08382500	Comparable median Gallinas Creek discharge (1951-2022)
Unit	km	m	m ³ /s	m ³ /s	m ³ /s	m ³ /s
7/15/2022	11.60	1433.68	5.10	0.82	0.85	0.05
7/29/2022	3.36	1434.77	8.69	1.93	1.56	0.23
8/19/2022	7.89	1432.51	13.08	0.99	4.13	0.20
10/12/2022	7.62	1435.83	4.59	0.57	0.08	0.00

The longitudinal data in Figure 11 show a clear propagation of the wildfire disturbances observed in Gallinas Creek, and a transition in water quality parameters between lotic and lentic systems. The associated delta region is also dynamic. For example, between July 29 and October 12, 2022, the delta moved ~1.2 km upstream as the lake’s elevation rose by 3.31m. We did not have data for the delta for July 15, 2022, and July 29, 2022, due to logistical challenges. We observed DO reaching anoxic conditions (~0 mg/L) on August 19, 2022, near the delta region located 175 km downstream of the Gallinas EV long sampling site, located near the burn scar. The monitored sections featured floating debris and foamy water following monsoon precipitation events. The early run and the post-monsoon season DO concentrations remained > 5mg/L, suggesting that DO sags were triggered by runoff draining the Gallinas Creek watershed (~31% of total discharge near the Lake) and Pecos watershed (~69% of total discharge). Above the delta, we observed lower conductivity, pH, and temperature compared to the data from Santa Rosa Lake, and higher turbidity and DO values.

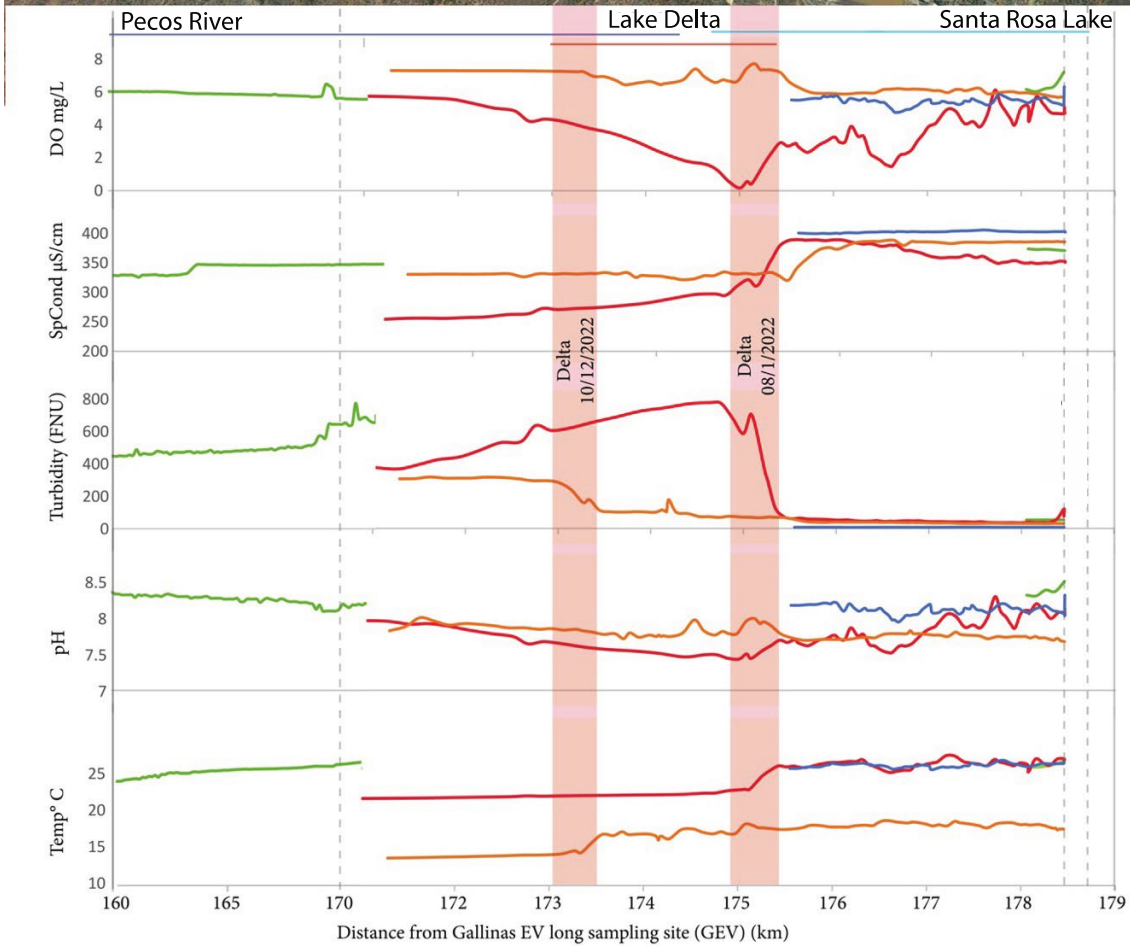
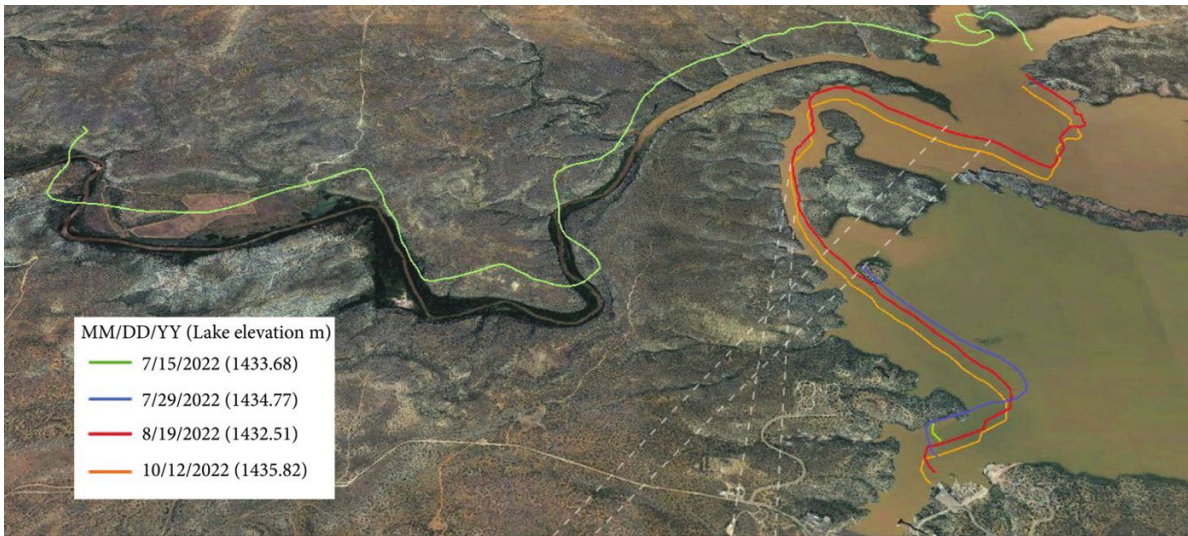
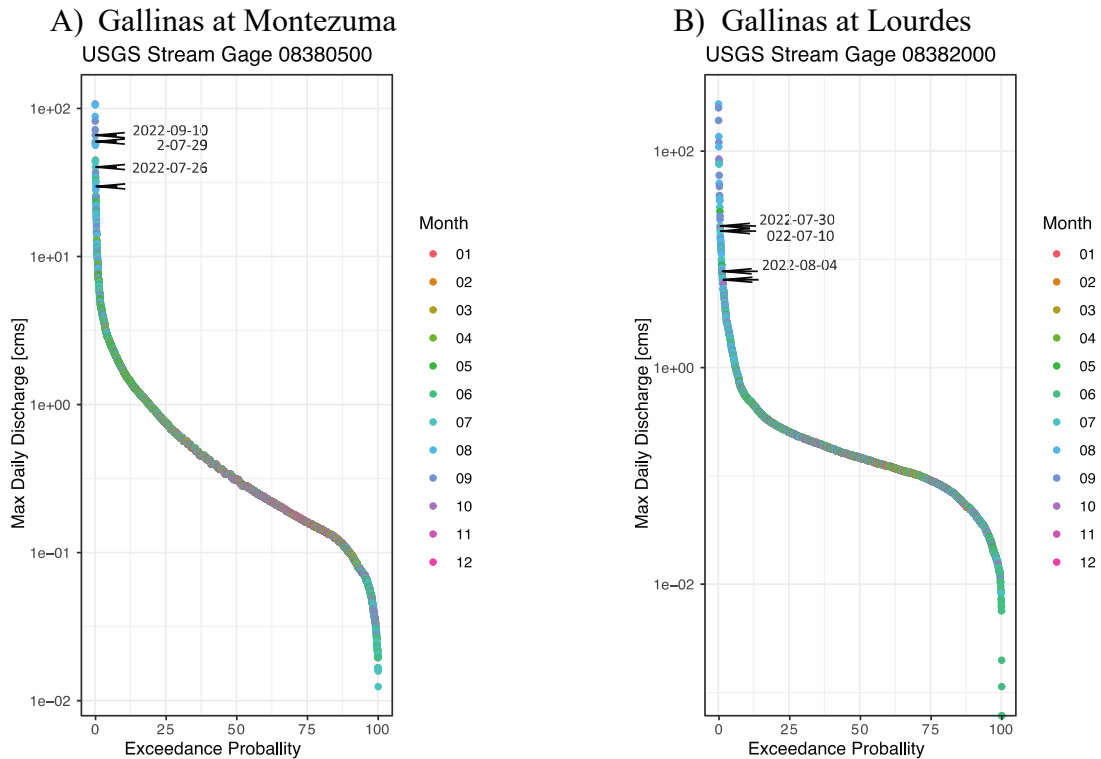


Figure 11. Lagrangian data of DO, specific conductivity, turbidity, pH, and water temperature collected with The Navigator. Data were collected during the monsoon period (green, blue, and red) and post-monsoon (orange). The red zone indicates the delta, which shifted as the lake level rose from 1432.51m to 1435.82m.

4. PRINCIPAL FINDINGS, CONCLUSIONS, AND RECOMMENDATIONS

4.1. Disturbance effects on surface water quality in streams and rivers

The discharge events during the 2022 monsoon season produced high discharge events at a greater frequency than pre-wildfire historical records within the upper Gallinas watershed (Figure 5). For example, the three highest discharge events recorded at GMZ during the 2022 monsoon season had exceedance probabilities of less than 0.15% and recurrence intervals greater than two years (Figure 12). Concurrent with high discharge events was a significant increase in turbidity and fDOM, which has been linked to the mobilization of sediments and organic material from burned watersheds (Figure 5) (Sherson et al. 2015; Ice, Neary, and Adams 2004; Smith et al. 2011).



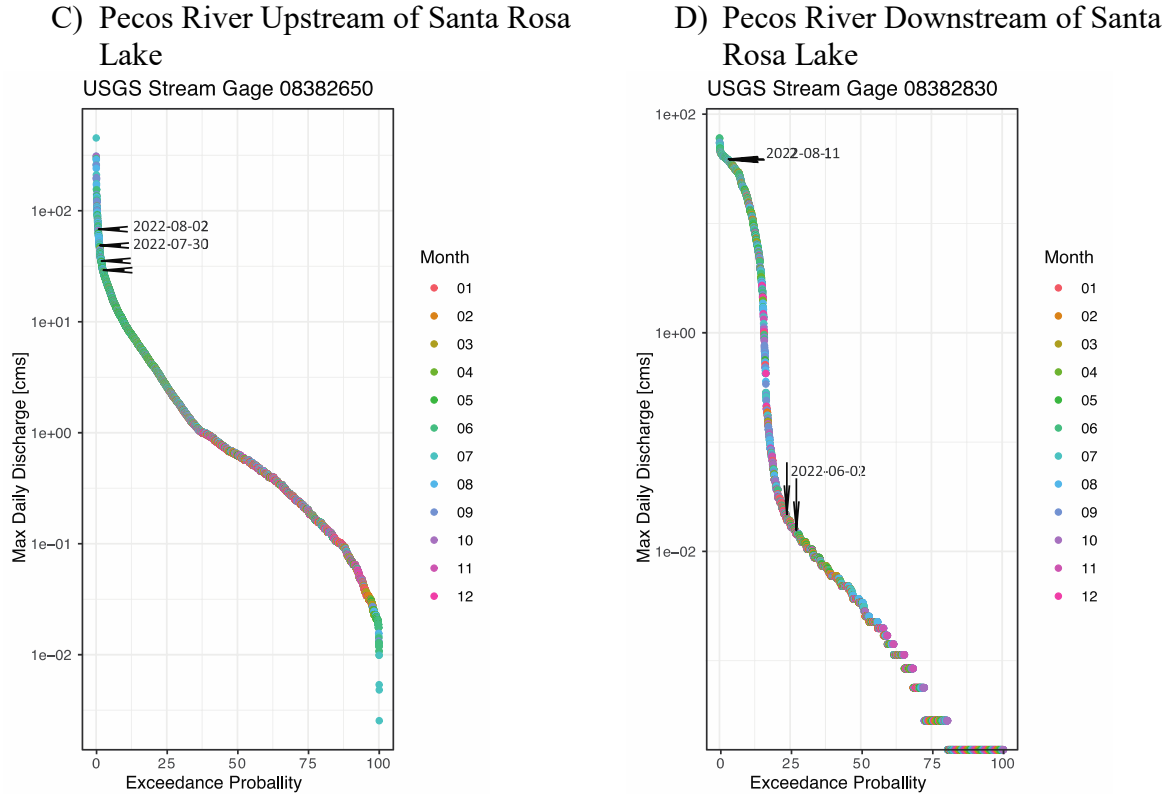


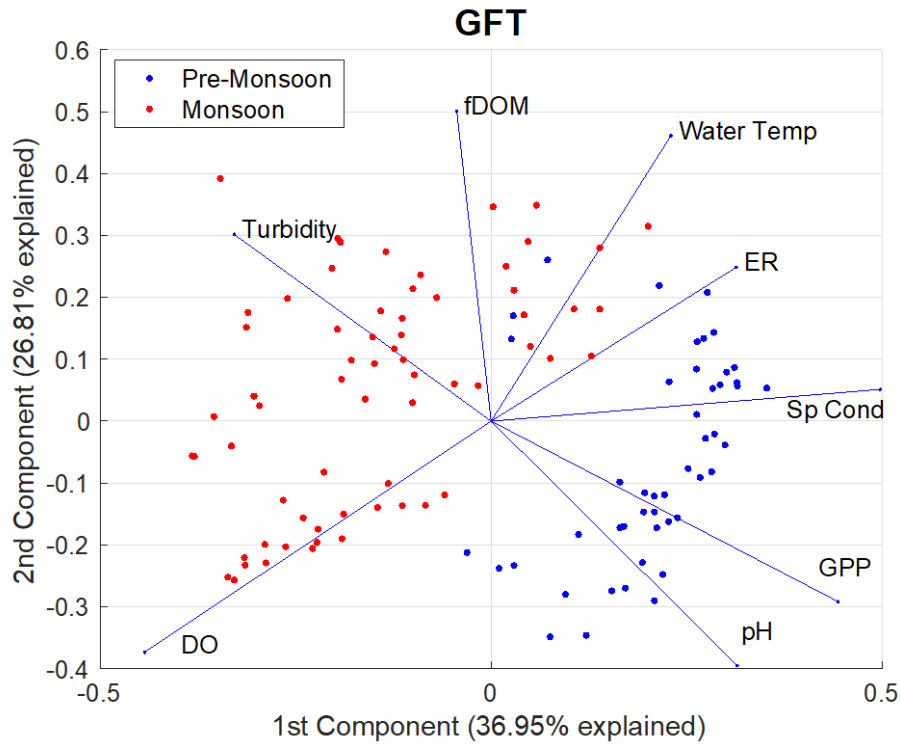
Figure 12. Exceedance probability plots for A) Gallinas at Montezuma, B) Gallinas at Lourdes, C) Pecos River Upstream of Santa Rosa Lake, and D) Pecos River Downstream of Santa Rosa Lake. The four highest discharge events in 2022 are annotated on the plot.

Dissolved oxygen sags were observed across all monitoring sites upstream of Santa Rosa Lake during high discharge events. However, the dissolved oxygen sags were not significant enough to cause hypoxia (i.e., dissolved oxygen less than 2 ppm) at any of the monitoring sites (Figure 5). The dissolved oxygen sags can be contributed to an increase in biological oxygen demand and heterotrophic respiration during high discharge events with the increase in dissolved organics within the water column (Saraceno et al. 2009; Regier et al. 2020; Bhurtun et al. 2019).

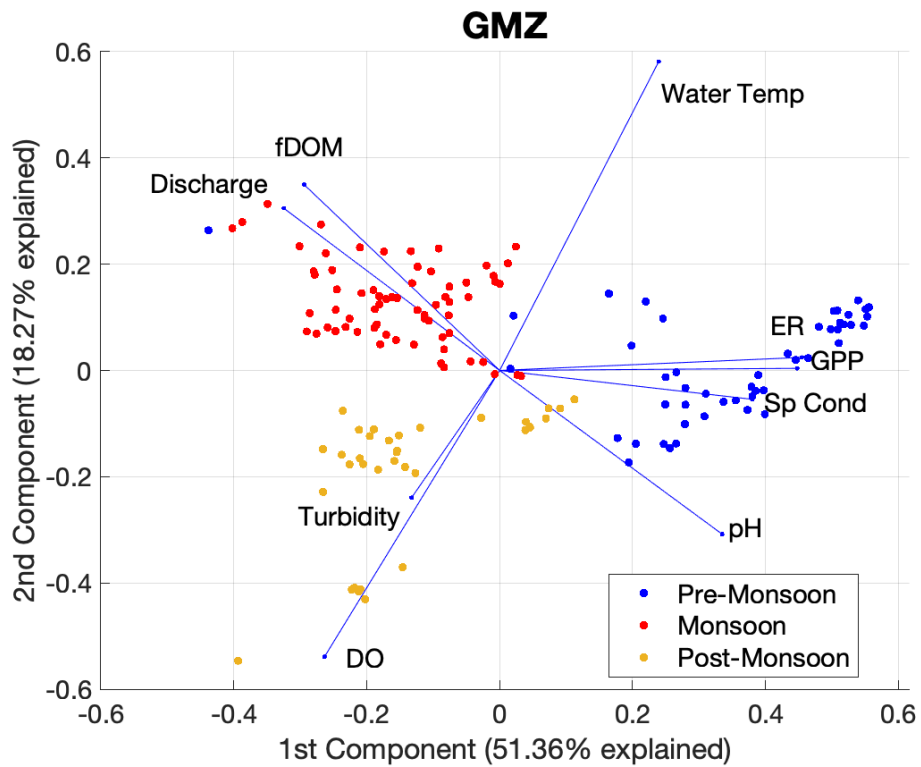
Principal component analysis demonstrates distinct monsoon period clustering at sites above Santa Rosa Lake, with discharge, fDOM, and turbidity being dominant variables, except for GMZ where turbidity is dominant in the post-monsoon period (Figure 13). The shift in GMZ principal component analysis is likely due to the large turbidity spikes following an increase in discharge of $6.8 \text{ m}^3\text{s}^{-1}$ on October 23, 2022, which produced turbidity values that exceeded those observed during the monsoon period. Unlike the other sites, the PBS site does not have distinct

temporal clusters in its PCA biplot, indicating that the variability between periods was less significant downstream of Santa Rosa Lake (Figure 13).

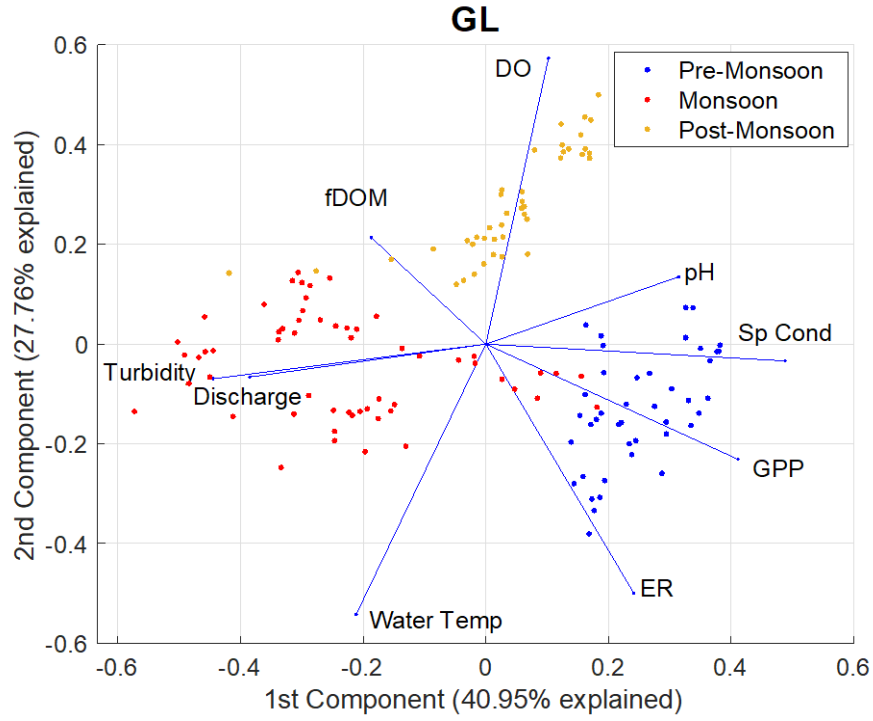
A)



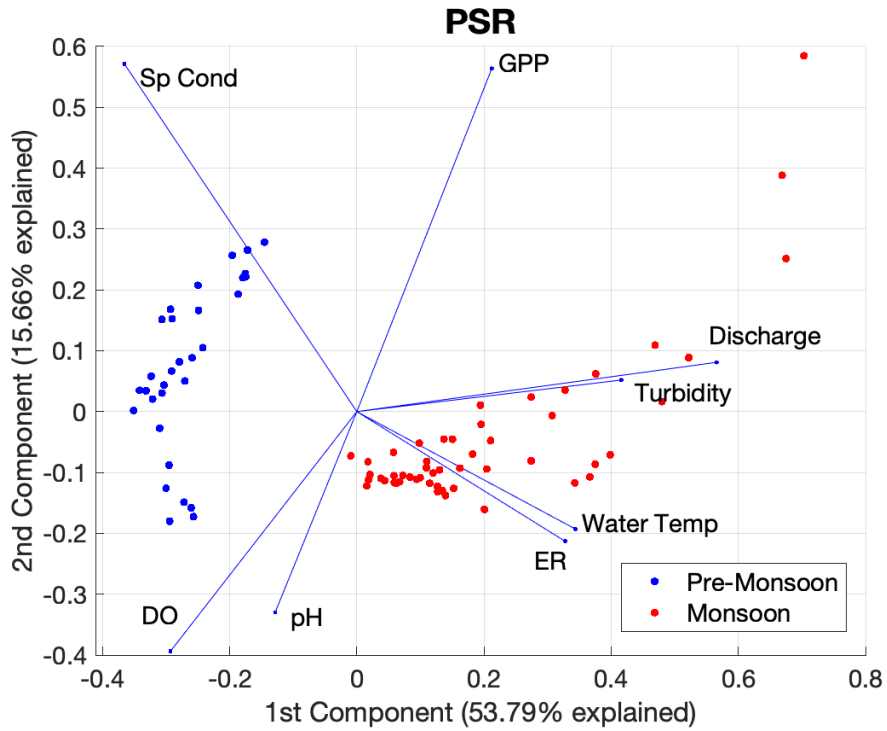
B)



C)



D)



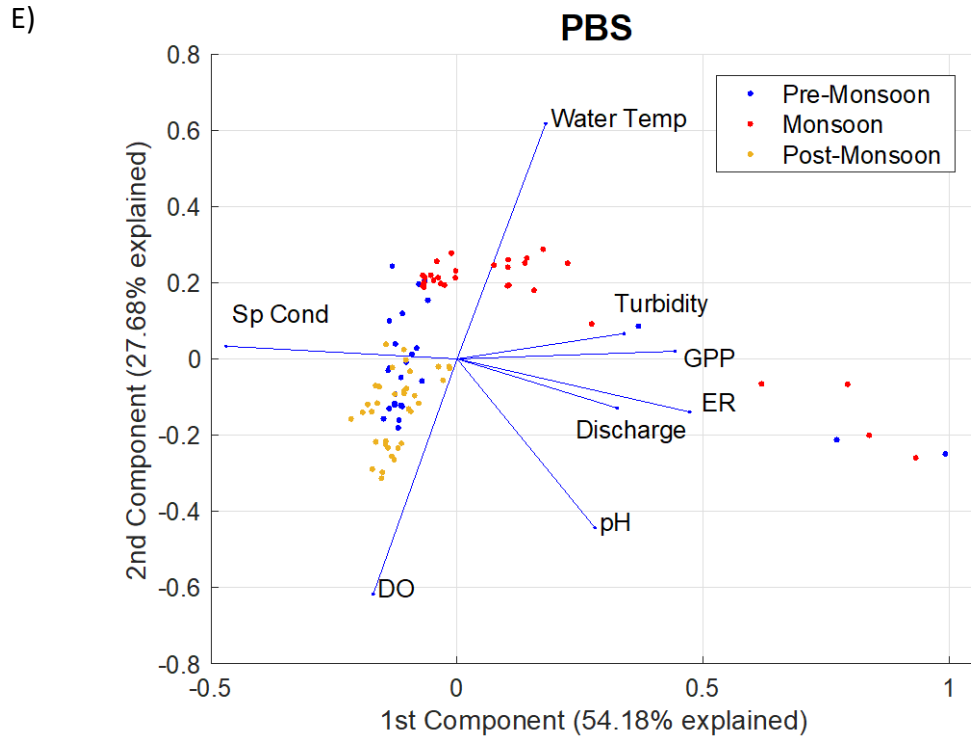


Figure 13. Principal component analysis at each sonde site from April 26, 2022, to November 8, 2022. A) Gallinas Creek near Gallinas, B) Gallinas Creek near Montezuma, C) Gallinas Creek near Lourdes, D) Pecos River upstream of Santa Rosa Lake, and E) Pecos River downstream of Santa Rosa Lake.

4.2. Disturbance effects on stream metabolism

From the onset of the monsoon season, there was a significant reduction of GPP at GFT, GMZ, and GL, with GFT and GMZ gross primary production nearing $0 \text{ gO}_2 \text{ m}^{-2} \text{ d}^{-1}$ for a majority of the monsoon period (Figure 6). With the exception for PSR and PBS, principal component analysis shows a strong negative relationship between GPP, and discharge and turbidity (Figure 13). The reduction in GPP may be attributed to scouring of the streambed, thus mobilizing phototrophic communities (Chin et al. 2019; Sherson et al. 2015). Scouring of the streambed would also support the overall reduction in ER at the GFT, GMZ, and GL sites due to phototrophic and heterotrophic communities being collocated on the streambed (Krause et al. 2017; Wondzell 2011). The PSR and PBS sites did not experience a significant reduction in GPP during the monsoon period due to low ambient production during the pre-monsoon season (Figure 6). Unlike the other sites, PSR and PBS experienced an increase in ER during the monsoon season, which may indicate increased dissolved organics at the two sub-reaches (Hensley et al. 2019; Bernhardt et al. 2018).

The reduction of GPP during the monsoon and post-monsoon season could reduce the capacity of the Gallinas River to retain nutrients. Past publications have shown a direct relationship between nutrient uptake and GPP due to inorganic nutrients ammonium, nitrate, and phosphate being fundamental building block to phototrophic cell growth. With the reduction in GPP, ecosystem services that increase nutrient retention can be diminished, allowing for a higher percentage of nutrients to be transported to downstream reaches and reservoirs. The reduction of GPP and ER during the monsoon season was less substantial at GL and PSR, and unlike any other monitoring sites, both increased concurrently with a high discharge event from a controlled release at Santa Rosa Dam (Figures 5 and 13). Discharge events during the 2022 monsoon season did not vary significantly from historical peak discharge events at the GL, PSR, and PBS sites, with the highest discharge events producing exceedance probabilities of 0.60%, 0.74%, and 0.65%, respectively (Figure 12). Therefore, streambed scouring at GL, PSR, and PBS may have been less severe than that experienced at GFT and GMZ, thus decreasing the impact to the localized benthic communities.

4.3. Disturbance effects on lakes, and lake controls on propagation of disturbances

Our Lagrangian data provide insights about how water disturbances sourced in burned areas propagate into the Pecos River and Santa Rosa Lake, which could not be inferred from fixed (Eulerian) monitoring or coarse spatial profiling (Hensley et al. 2020). We observed hyperpycnal flow formation when river flows with higher density joined lake water with lower densities. In hyperpycnal flows, the incoming flow plunges and generates highly dynamic and even long-lived dense underflows (Zavala 2020). For example, turbidity values drastically changed from ~700 FNU (~22 °C water temperature) to ~60 FNU (~26 °C water temperature) within a short distance of ~0.25 km on August 19, 2022. Similarly, on October 12, 2022, turbidity changed from ~300 FNU (~14 °C water temperature) to ~100 FNU (~18 °C water temperature) within 0.3 km, generating an underflow (Figures 14 and 15).

The data strongly suggest that the wildfire disturbances generated downwelling cycles and, consequently, should have increased sediment deposition into the lake's bed even though we did not have depth profile data to quantify deposition rates. Furthermore, we saw floating debris accumulating on the plunge point, confirming the presence of underflows with high-density sediments and upper flows with lighter materials (Figure 15).

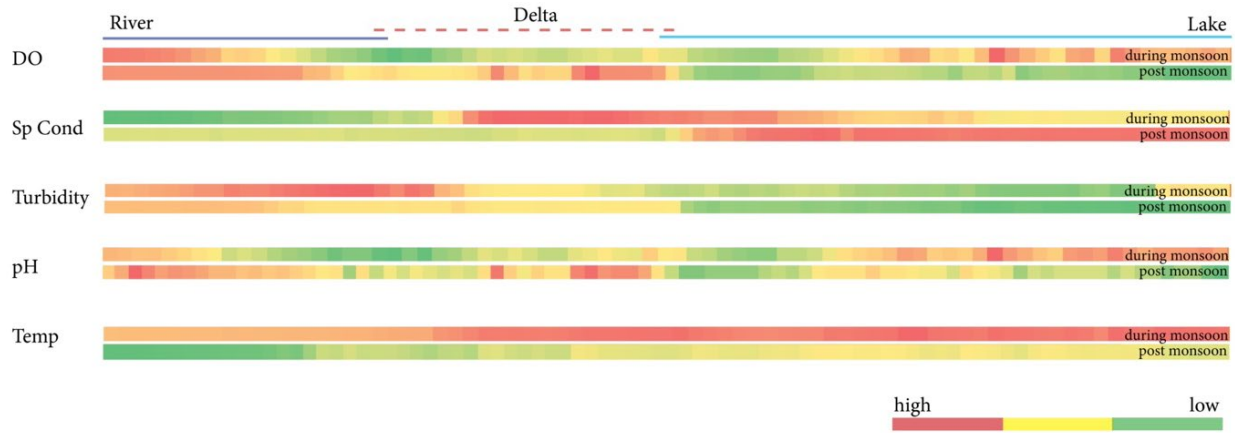


Figure 14. Heatmap of the water quality parameters highlighting hotspots near delta region. The horizontal line indicates river-like dominant conditions, the delta, and the lake.

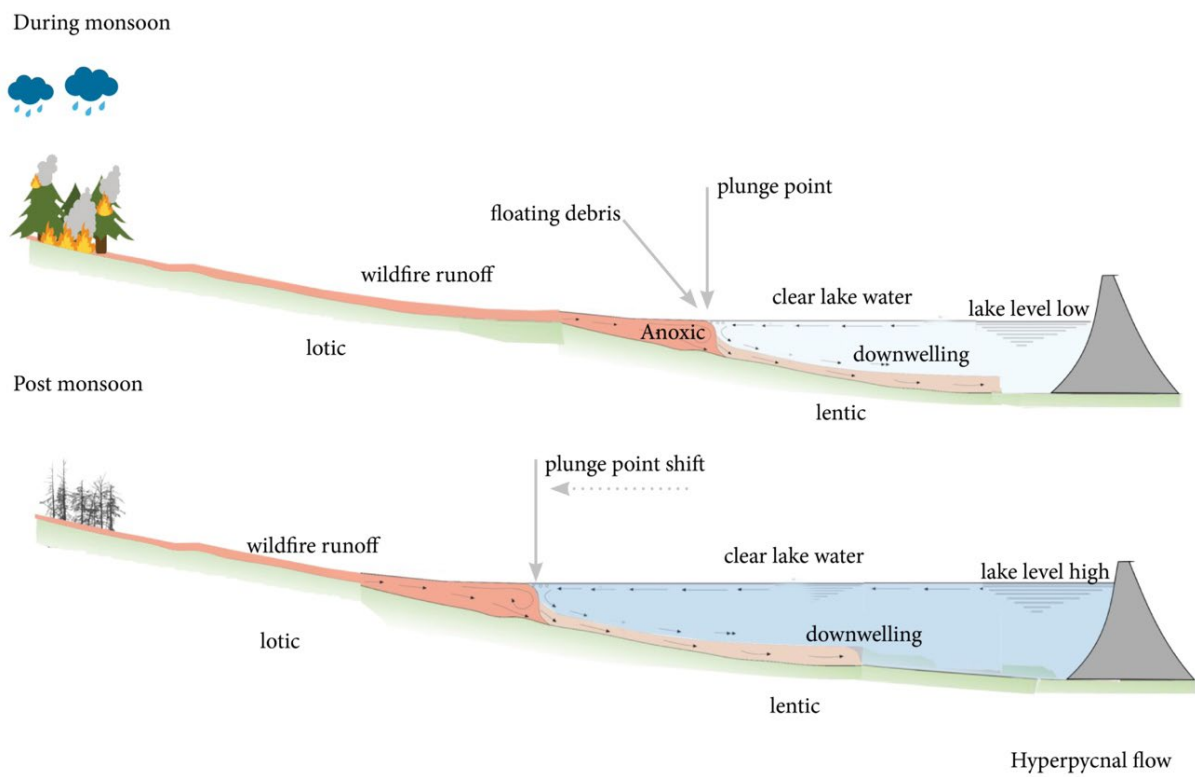


Figure 15. Conceptual diagram comparing monsoon and post-monsoon hyperpycnal flows based on sensor data.

The Lagrangian monitoring over the monsoon seasons showed that water quality parameters changed more over space than over time. This helped us identify so-called hotspots, which were associated with changing conditions from lotic to lentic systems. As expected, higher

temperatures in the lake could be associated with increased residence times. However, it is important to notice that shallower depths in the river were, counterintuitively, not associated with increased water temperatures, suggesting a more dominant role of absorption of solar radiation due to the presence of increased sediments and debris in the lake.

DO variations in aquatic ecosystems are largely influenced by aquatic metabolism and re-aeration. GPP and ER increase with biomass, ER increases with organic matter, and GPP is limited by sunlight availability, which decreases with turbidity (Nichols et al. 2022; Summers et al. 2020). Therefore, it is likely that the excess organic material draining from the burned areas and propagating into the delta may have induced increased ER and reduced GPP, resulting in anoxic conditions.

4.4. Disturbance effects on communities

Wildfires are increasing in severity and intensity across the southwestern United States, affecting the water quality of streams, rivers, lakes, and aquifers. Ash produced by wildfire has trace elements, nutrients, and other contaminants. After a wildfire, these contaminants are released during precipitation events and propagate through fluvial networks. The elevated nutrients in surface water resources are detrimental to human health and are also associated with eutrophication events altering aquatic ecosystems. To understand post-fire water quality dynamics, the study of nutrient concentrations in streams is extremely important but limited studies have been conducted on demand, soon after a wildfire begins. Evaluating the current data, most of the nutrients were observed to be high in concentration during the monsoon season as many nutrients from the burn scar area are released into surface waters during the post-fire rainfall events. The increased nutrient loading and contamination in surface waters pose a high risk to water supplies, thus, effective water treatment strategies and procedures should be adopted to mitigate the risk associated with consumer health.

The Gallinas River watershed is the primary source of drinking water for the city of Las Vegas, New Mexico. The impacts of the increased turbidity from ash and sediment impact the drinking water supply as the city does not have the ability to treat the water that has an increased sediment load. This impacts around 17,000 residents who rely on the water from Gallinas Creek. Current interim measures, such as flood control structures and a pre-treatment system, have allowed for the city to build a 49-day treatable water supply in their reservoirs. However, the impact of the wildfire is expected to be seen for many years while Las Vegas pursues its plans to

upgrade the Las Vegas water system to adequately treat the water in the future (Davis 2022; Fendt 2022).

Monitoring water quality in near real-time can provide invaluable information that will allow communities to take action needed to protect their drinking water source in rapidly evolving situations, such as during and after wildfires. Beyond the Hermit's Peak/Calf Canyon wildfire, the successful implementation of monitoring networks using rapid response techniques can provide a framework for investigating the effects of other disturbance events and their downstream impacts.

5. REFERENCES

- Abatzoglou, John T., and A. Park Williams. 2016. "Impact of Anthropogenic Climate Change on Wildfire across Western US Forests." *Proceedings of the National Academy of Sciences of the United States of America* 113 (42): 11770–75. <https://doi.org/10.1073/pnas.1607171113>.
- Abram, Nerilie J., Michael K. Gagan, Malcolm T. McCulloch, John Chappell, and Wahyoe S. Hantoro. 2003. "Coral Reef Death during the 1997 Indian Ocean Dipole Linked to Indonesian Wildfires." *Science* 301 (5635): 952–55.
- Adams, Mark A. 2013. "Mega-Fires, Tipping Points and Ecosystem Services: Managing Forests and Woodlands in an Uncertain Future." *Forest Ecology and Management, The Mega-fire reality*, 294 (April): 250–61. <https://doi.org/10.1016/j.foreco.2012.11.039>.
- Appling, Alison P., Robert O. Hall, Charles B. Yackulic, and Maite Arroita. 2018. "Overcoming Equifinality: Leveraging Long Time Series for Stream Metabolism Estimation." *Journal of Geophysical Research: Biogeosciences* 123 (2): 624–45. <https://doi.org/10.1002/2017JG004140>.
- Ball, Grady, Peter Regier, Ricardo González-Pinzón, Justin Reale, and David Van Horn. 2021. "Wildfires Increasingly Impact Western US Fluvial Networks." *Nature Communications* 12 (1). <https://doi.org/10.1038/s41467-021-22747-3>.
- Bernhardt, Emily S., James B. Heffernan, Nancy B. Grimm, Emily H. Stanley, Judson W. Harvey, Maite Arroita, Alison P. Appling, et al. 2018. "The Metabolic Regimes of Flowing Waters." *Limnology and Oceanography* 63 (S1): S99–118. <https://doi.org/10.1002/lno.10726>.
- Bhurtun, Pratima, Ludovic Lesven, Cyril Ruckebusch, Cédric Halkett, Jean-Paul Cornard, and Gabriel Billon. 2019. "Understanding the Impact of the Changes in Weather Conditions on Surface Water Quality." *Science of The Total Environment* 652 (February): 289–99. <https://doi.org/10.1016/j.scitotenv.2018.10.246>.
- Bladon, Kevin D., Monica B. Emelko, Uldis Silins, and Micheal Stone. 2014. "Wildfire and the Future of Water Supply." *Environmental Science & Technology* 48 (16): 8936–43. <https://doi.org/10.1021/es500130g>.
- Calkin, David E., Matthew P. Thompson, and Mark A. Finney. 2015. "Negative Consequences of Positive Feedbacks in US Wildfire Management." *Forest Ecosystems* 2 (1): 9. <https://doi.org/10.1186/s40663-015-0033-8>.
- Chin, Anne, Anna P. Solverson, Alison P. O'Dowd, Joan L. Florsheim, Alicia M. Kinoshita, Samira Nourbakhshbeidokhti, Samantha M. Sellers, Lauren Tyner, and Rachel Gidley. 2019. "Interacting Geomorphic and Ecological Response of Step-Pool Streams after Wildfire." *GSA Bulletin* 131 (9–10): 1480–1500. <https://doi.org/10.1130/B35049.1>.
- Dahm, Clifford N., Roxanne I. Candelaria-Ley, Chelsea S. Reale, Justin K. Reale, and David J. Van Horn. 2015. "Extreme Water Quality Degradation Following a Catastrophic Forest Fire." *Freshwater Biology* 60 (12): 2584–99. <https://doi.org/10.1111/fwb.12548>.

- Davies, Ian P., Ryan D. Haugo, James C. Robertson, and Phillip S. Levin. 2018. "The Unequal Vulnerability of Communities of Color to Wildfire." Edited by Julia A. Jones. *PLOS ONE* 13 (11): e0205825. <https://doi.org/10.1371/journal.pone.0205825>.
- Davis, Theresa. 2022. "Fire Could Impact Las Vegas Water System for Years - Albuquerque Journal." 2022. <https://www.abqjournal.com/2523742/fire-could-impact-las-vegas-water-system-for-years.html>.
- Downing, Bryan D., Brian A. Pellerin, Brian A. Bergamaschi, John Franco Saraceno, and Tamara E.C. Kraus. 2012. "Seeing the Light: The Effects of Particles, Dissolved Materials, and Temperature on In Situ Measurements of DOM Fluorescence in Rivers and Streams: Effects and Compensation for In Situ DOM Fluorescence." *Limnology and Oceanography: Methods* 10 (10): 767–75. <https://doi.org/10.4319/lom.2012.10.767>.
- Fendt, Lindsay. 2022. "The Fire and Flood next Time." Searchlight New Mexico. October 21, 2022. <http://searchlightnm.org/the-fire-and-flood-next-time/>.
- Hensley, Robert T., Lily Kirk, Margaret Spangler, Michael N. Gooseff, and Matthew J. Cohen. 2019. "Flow Extremes as Spatiotemporal Control Points on River Solute Fluxes and Metabolism." *Journal of Geophysical Research: Biogeosciences* 124 (3): 537–55. <https://doi.org/10.1029/2018JG004738>.
- Hensley, Robert T., Margaret J. Spangler, Lauren F. DeVito, Paul H. Decker, Matthew J. Cohen, and Michael N. Gooseff. 2020. "Evaluating Spatiotemporal Variation in Water Chemistry of the Upper Colorado River Using Longitudinal Profiling." *Hydrological Processes* 34 (8): 1782–93. <https://doi.org/10.1002/hyp.13690>.
- Ice, George G., Daniel G. Neary, and Paul W. Adams. 2004. "Effects of Wildfire on Soils and Watershed Processes." *Journal of Forestry* 102 (6): 16–20. <https://doi.org/10.1093/jof/102.6.16>.
- Jolliffe, Ian T., and Jorge Cadima. 2016. "Principal Component Analysis: A Review and Recent Developments." *Philosophical Transactions of the Royal Society A: Mathematical, Physical and Engineering Sciences* 374 (2065): 20150202. <https://doi.org/10.1098/rsta.2015.0202>.
- Kincheon, James. 1959. "Flow-Duration Curves." Water Supply Paper 1542-A. USGS. <https://doi.org/10.3133/wsp1542A>.
- Krause, Stefan, Jörg Lewandowski, Nancy B. Grimm, David M. Hannah, Gilles Pinay, Karlie McDonald, Eugènia Martí, et al. 2017. "Ecohydrological Interfaces as Hot Spots of Ecosystem Processes: ECOHYDROLOGICAL INTERFACES AS HOT SPOTS." *Water Resources Research* 53 (8): 6359–76. <https://doi.org/10.1002/2016WR019516>.
- LeComte, Douglas. 2023. "U.S. Weather Highlights 2022—Drought, Flash Floods, Severe Outbreaks, Hurricane Ian, Blockbuster Winter Storms." *Weatherwise* 76 (3): 14–22. <https://doi.org/10.1080/00431672.2023.2180974>.
- Meek, David W., Jerry L. Hatfield, Terry A. Howell, Sherwood B. Idso, and Robert J. Reginato. 1984. "A Generalized Relationship between Photosynthetically Active Radiation and Solar Radiation 1." *Agronomy Journal* 76 (6): 939–45. <https://doi.org/10.2134/agronj1984.00021962007600060018x>.

- Nichols, Justin, Aashish Sanjay Khandelwal, Peter Regier, Betsy Summers, David J. Van Horn, and Ricardo González-Pinzón. 2022. “The Understudied Winter: Evidence of How Precipitation Differences Affect Stream Metabolism in a Headwater.” *Frontiers in Water* 4 (September): 1003159. <https://doi.org/10.3389/frwa.2022.1003159>.
- North, Malcom P., Scott L. Stephens, Brandon M. Collins, James K. Agee, Gregory H. Aplet, Jerry F. Franklin, and Peter Z. Fulé. 2015. “Reform Forest Fire Management.” *Science* 349 (6254): 1280–81. <https://doi.org/10.1126/science.aab2356>.
- Odum, Howard T. 1956. “Primary Production in Flowing Waters.” *Limnology and Oceanography* 1 (2): 102–17. <https://doi.org/10.4319/lo.1956.1.2.0102>.
- Reale, Justin K., David J. Van Horn, Katherine E. Condon, and Clifford N. Dahm. 2015. “The Effects of Catastrophic Wildfire on Water Quality along a River Continuum.” *Freshwater Science* 34 (4): 1426–42. <https://doi.org/10.1086/684001>.
- Regier, Peter J., Ricardo González-Pinzón, David J. Van Horn, Justin K. Reale, Justin Nichols, and Aashish Khandewal. 2020. “Water Quality Impacts of Urban and Non-Urban Arid-Land Runoff on the Rio Grande.” *Science of The Total Environment* 729 (August): 138443. <https://doi.org/10.1016/j.scitotenv.2020.138443>.
- Saraceno, John Franco, Brian A. Pellerin, Bryan D. Downing, Emmanuel Boss, Philip A.M. Bachand, and Brian A. Bergamaschi. 2009. “High-Frequency In Situ Optical Measurements during a Storm Event: Assessing Relationships between Dissolved Organic Matter, Sediment Concentrations, and Hydrologic Processes.” *Journal of Geophysical Research* 114 (December). <https://doi.org/10.1029/2009jg000989>.
- Sherson, Lauren R., David J. Van Horn, Jesus D. Gomez-Velez, Laura J. Crossey, and Clifford N. Dahm. 2015. “Nutrient Dynamics in an Alpine Headwater Stream: Use of Continuous Water Quality Sensors to Examine Responses to Wildfire and Precipitation Events.” *Hydrological Processes* 29 (14): 3193–3207. <https://doi.org/10.1002/hyp.10426>.
- Smith, Hugh G., Gary J. Sheridan, Patrick N.J. Lane, Petter Nyman, and Shane Haydon. 2011. “Wildfire Effects on Water Quality in Forest Catchments: A Review with Implications for Water Supply.” *Journal of Hydrology* 396 (1): 170–92. <https://doi.org/10.1016/j.jhydrol.2010.10.043>.
- Summers, Betsy M., David J. Van Horn, Ricardo González-Pinzón, Rebecca J. Bixby, Michael R. Grace, Lauren R. Sherson, Laura J. Crossey, et al. 2020. “Long-Term Data Reveal Highly-Variable Metabolism and Transitions in Trophic Status in a Montane Stream.” *Freshwater Science* 39 (2): 241–55. <https://doi.org/10.1086/708659>.
- Thermo Fisher Scientific Inc., 2015, <https://assets.thermofisher.com/TFS-Assets/CMD/manuals/PI-D09161-DA-Ammonia-DIC-PID09161-EN.pdf>, <https://assets.thermofisher.com/TFS-Assets/CMD/manuals/PI-D09244-DA-Phosphate-PID09244-EN.pdf>, <https://assets.thermofisher.com/TFS-Assets/CMD/manuals/PI-D06736-DA-Sulphate-PID06736-EN.pdf>, <https://assets.thermofisher.com/TFS-Assets/CMD/manuals/PI-D09228-DA-TON-Hydrazine-Nitrate-PID09228-EN.pdf>.
- Thermo Fisher Scientific Inc., 2018, <https://assets.thermofisher.com/TFS-Assets/CMD/Application-Notes/AN-71728-DA-ISO-Water-Pollutants-AN71728-EN.pdf>.

- Tunby, Paige. 2022. "Rapid Response Protocol (RRP) for Monitoring Water Quality Parameters for Wildfire Disturbance." *Civil Engineering ETDs*, July. https://digitalrepository.unm.edu/ce_etds/267.
- Wagner, Richard J., Robert W. Boulger Jr., Carolyn J. Oblinger, and Brett A. Smith. 2006. "Guidelines and Standard Procedures for Continuous Water-Quality Monitors: Station Operation, Record Computation, and Data Reporting." <http://pubs.er.usgs.gov/publication/tm1D3>.
- Westerling, Anthony L., Benjamin P. Bryant, Haiganoush K. Preisler, Thomas P. Holmes, Hugo G. Hidalgo, Tapash Das, and Sudhir R. Shrestha. 2011. "Climate Change and Growth Scenarios for California Wildfire." *Climatic Change* 109 (1): 445–63. <https://doi.org/10.1007/s10584-011-0329-9>.
- Wondzell, Steven M. 2011. "The Role of the Hyporheic Zone across Stream Networks." *Hydrological Processes* 25 (22): 3525–32. <https://doi.org/10.1002/hyp.8119>.
- Zavala, Carlos. 2020. "Hyperpycnal (over Density) Flows and Deposits." *Journal of Palaeogeography* 9 (1): 17. <https://doi.org/10.1186/s42501-020-00065-x>.